

# A city-scale estimation of rooftop solar photovoltaic potential based on deep learning

Teng Zhong<sup>a,b,c,1</sup>, Zhixin Zhang<sup>a,b,c,1</sup>, Min Chen<sup>a,b,c,g,\*</sup>, Kai Zhang<sup>a,b,c</sup>, Zixuan Zhou<sup>a,b,c</sup>, Rui Zhu<sup>d</sup>, Yijie Wang<sup>a,b,c</sup>, Guonian Lü<sup>a,b,c</sup>, Jinyue Yan<sup>e,f</sup>

<sup>a</sup> Key Laboratory of Virtual Geographic Environment (Ministry of Education of PRC), Nanjing Normal University, Nanjing 210023, China

<sup>b</sup> State Key Laboratory Cultivation Base of Geographical Environment Evolution, Nanjing 210023, China

<sup>c</sup> Jiangsu Center for Collaborative Innovation in Geographical Information Resource Development and Application, Nanjing 210023, China

<sup>d</sup> Senseable City Laboratory, Future Urban Mobility IRG, Singapore-MIT Alliance for Research and Technology, 1 Create Way, 09-02 Create Tower, 138062, Singapore

<sup>e</sup> School of Business, Society & Engineering, Mälardalen University, Västerås 721223, Sweden

<sup>f</sup> Department of Chemical Engineering, KTH Royal Institute of Technology, Stockholm 10044, Sweden

<sup>g</sup> Jiangsu Provincial Key Laboratory for NSLSCS, School of Mathematical Science, Nanjing Normal University, Nanjing 210023, China

## HIGHLIGHTS

- A framework for city-scale rooftop solar PV potential estimation was developed.
- Labor cost of deep learning was significantly reduced with proposed spatial optimization sampling strategy.
- Rooftop extraction model was proved to be robust in districts with different architectural styles and land use.
- 311,853 GWh rooftop solar PV potential was estimated for Nanjing in 2019.
- 330.36 km<sup>2</sup> rooftop area and 66 GW installed capacity were estimated for Nanjing.

## ARTICLE INFO

### Keywords:

rooftop solar photovoltaic (PV) potential  
geographic information systems (GIS)  
Deep learning  
Sampling strategy  
City-scale

## ABSTRACT

The estimation of rooftop solar photovoltaic (PV) potential is crucial for policymaking around sustainable energy plans. But it is difficult to accurately estimate the availability of rooftop area for solar radiation on a city-scale. In this study, a generic framework for estimating the rooftop solar PV potential on a city-scale using publicly available high-resolution satellite images is proposed. A deep learning-based method is developed to extract the rooftop area with image semantic segmentation automatically. A spatial optimization sampling strategy is developed to solve the labor-intensive problem when training the rooftop extraction model based on prior knowledge of urban and rural spatial layout and land use. In the case study of Nanjing, China, the labor cost on preparing the dataset for training the rooftop extraction model has been reduced by about 80% with the proposed spatial optimization sampling strategy. Meanwhile, the robustness of the rooftop extraction model in districts with different architectural styles and land use has been improved. The total rooftop area extracted was 330.36 km<sup>2</sup>, and the overall accuracy reached 0.92. The estimation results show that Nanjing has significant potential for rooftop-mounted PV installations, and the potential installed capacity reached 66 GW. The annual rooftop solar PV potential was approximately 311,853 GWh, with a corresponding estimated power generation of 49,897 GWh in 2019.

## 1. Introduction

As an emerging renewable energy technology, solar photovoltaic

(PV) technology is recognized as an essential option for sustainable energy transformation [1]. In recent years, benefiting from the advancement of technology, the reduction of material costs, and the

\* Corresponding author at: School of Geography, Nanjing Normal University, NO.1 Wenyuan Road, Qixia District, Nanjing 210023, PR China.

E-mail address: [chenmin0902@njnu.edu.cn](mailto:chenmin0902@njnu.edu.cn) (M. Chen).

<sup>1</sup> Both authors contributed equally to this study.

government's support for electricity production from renewable energy, solar PV technology has been increasingly developed [2]. Especially in China, the world's largest PV modules manufacturer, PV modules' production costs have been continuously reduced because of the continuous development and innovation of crystalline silicon solar cells [3]. A series of national incentive policies and regulations issued by the Chinese government has also actively promoted the scale development of China's domestic PV market, such as the 'Renewable energy law' and 'Benchmark feed-in tariff' [4]. With the development of technology and policies' support, China has become the world's largest market for solar PV power generation. The new installed capacity and cumulative installed capacity in China reached 53 GW and 130 GW, respectively in 2017, ranking the highest in the world [5]. In addition, in terms of grid parity capabilities and investment values of solar PVs, China's industrial and commercial solar PV systems have generated electricity at a lower cost than that of the grid power supply [6].

With the transformation of China's economic structure, the tertiary industry's development shows that energy demand is increasingly dispersed [7]. The development of distributed PVs is the inevitable choice based on the actual national conditions and the lessons learned from centralized PVs [8]. rooftops have been selected as the main location for PV installation by identifying favorable solar positions to avoid the loss of distributed energy generation caused by transmission [9]. Especially in China, with its high urban population density, occupying no additional land is a huge advantage of small-scale rooftop applications [10]. A series of subsidy policies formulated by the Chinese government has led to the continuous development of distributed PV power generation in the residential and commercial sectors, but also to the problem of excessive fiscal funding [11]. In China, natural resources, energy demand, and economic levels vary significantly among regions. Therefore, it is necessary to reasonably evaluate the rooftop solar PV potential before determining the scale of subsidies to help decision-makers better formulate sustainable energy plans to avoid negative impacts.

To estimate the solar PV potential of rooftop, it is necessary to quantify the available rooftop area of buildings that can receive solar radiation. At present, there are no publicly accessible rooftop data for most areas. Therefore, there is a need to develop an acquisition method for city-scale rooftop information to promote the assessment of rooftop solar PV potential on a large scale. Current studies have applied three-dimensional (3D) spatial data, such as light detection and ranging (LiDAR) and digital surface models (DSMs), to extract rooftop information in urban areas [12]. However, the acquisition cost for 3D spatial data is not affordable when applied in studies on a large scale. Besides, the processing of 3D spatial data is labor-intensive and time-consuming.

The use of massive open data from public map services to assess urban environments is increasing [13]. Google Earth satellite (GES) images are open-access data sources with advantages in extensive coverage, fast update speed, and low acquisition costs [14]. The emerging deep learning-based image semantic segmentation method can address the challenges of the complexity of building shapes. On the one hand, deep learning provides an effective solution for the city-scale extraction of rooftop information from optical images [15]. The extraction results can further support the estimation of city-scale solar potential and power generation [16]. On the other hand, because deep learning-based methods require many computer resources and large-scale labeled data, such methods are considered to require a significant amount of time and labor costs to complete widespread promotion. Although most studies have reduced the time cost needed for applying deep learning-based methods from computer hardware [17–19], minimizing the labor cost input in a large-scale promotion scenario has not been well explored. This study aims to bridge this gap and discuss critical issues that affect the benefits of deep learning-based methods in a city-scale promotion. The rooftop image samples are collected with a strategic approach that can significantly reduce the sample size input without reducing the accuracy of the rooftop extraction model. Besides,

a cost-benefit analysis of the image training sample size and rooftop extraction model's performance is conducted to determine whether the image training sample size can maximize the input-output benefit of the deep learning-based image semantic segmentation method.

This study's main objective is to develop a low-cost generic framework for the city-scale extraction of building rooftop areas, which can serve as a data basis for the large-scale assessment of rooftop solar PV potential. A spatial optimization sampling strategy based on prior knowledge of urban and rural spatial layouts and land use is proposed to obtain training samples from GES images and further train the rooftop extraction model under the deep learning-based image semantic segmentation method. By applying this model, a case study in Nanjing, China, is implemented to illustrate the extraction of rooftops with the proposed framework, and the extracted rooftop area is then used to assess the rooftop solar PV potential and solar PV power generation of the rooftops in Nanjing in 2019.

## 2. Literature review

### 2.1. City-scale solar PV potential estimation

#### 2.1.1. Methods of city-scale solar PV potential estimation

Considerable efforts have been made to evaluate the global and regional solar energy potential in the existing studies, many of which have focused on the technological feasibility and economic feasibility of solar power PV generation [20,21]. However, it is still challenging to quickly apply the proposed method to a large-scale promotion while ensuring solar energy estimation accuracy. Traditional studies have applied various social factors, such as land use and the areas of buildings, to estimate the solar PV potential of a city [22,23]. These methods are effective when the building rooftop area data are not available; however, the solar potential estimation accuracy is limited. Because high-rise urban areas are not always suitable for installing solar PV panels, accurate estimates of the available rooftop area are of great significance for reliable solar potential estimation [24]. Levinson et al. used high-resolution orthophotos and LiDAR data in combination with vegetation growth models to estimate solar potential [25]. Ko et al. developed a novel algorithm by considering the effect of shadows, rooftop surface availability, rooftop features (i.e., chimneys or walls), and the azimuthal angle on the measurement of rooftop solar potential [26]. By considering the actual area of the available roof surface and the effect of shadow on the potential assessment, these methods obtain more accurate estimation results. However, these methods have high requirements for the quality and quantity of data, and their efficiency is low. These disadvantages make it challenging to extend these methods to studies of regions or more extensive scale estimation. Many studies have recently applied the Geographic Information System (GIS) to estimate solar PV potential on the city-scale [27,28]. The important distinction of the GIS method is that rooftop suitability is not determined by manually selecting buildings or using predetermined constant values [29]. The GIS method shows higher accuracy than the constant values method and allows handling of larger data sets than manual selection.

#### 2.1.2. Resources of city-scale solar PV potential estimation

In urban environments, the limitation of available areas for receiving solar radiation and sunlight blocking by high-rise buildings can prevent solar energy's full utilization [30]. Current city-scale objects for the assessment and study of potential solar resources include road pavement [31], noise barriers [32], and building rooftops [33]. For example, Hofierka et al. developed the v.sun model to simulate the spatial distribution of different parts of a building receiving solar radiation in Presov, Slovakia [34]. Jakubiec et al. proposed a method based on detailed 3D urban massing models to predict PV panels' citywide electricity revenue in Cambridge, Massachusetts [35]. Mohajeri et al. used a deep learning-based method to obtain building information from highly accurate LiDAR data to assess the solar PV potential of Geneva, Sweden

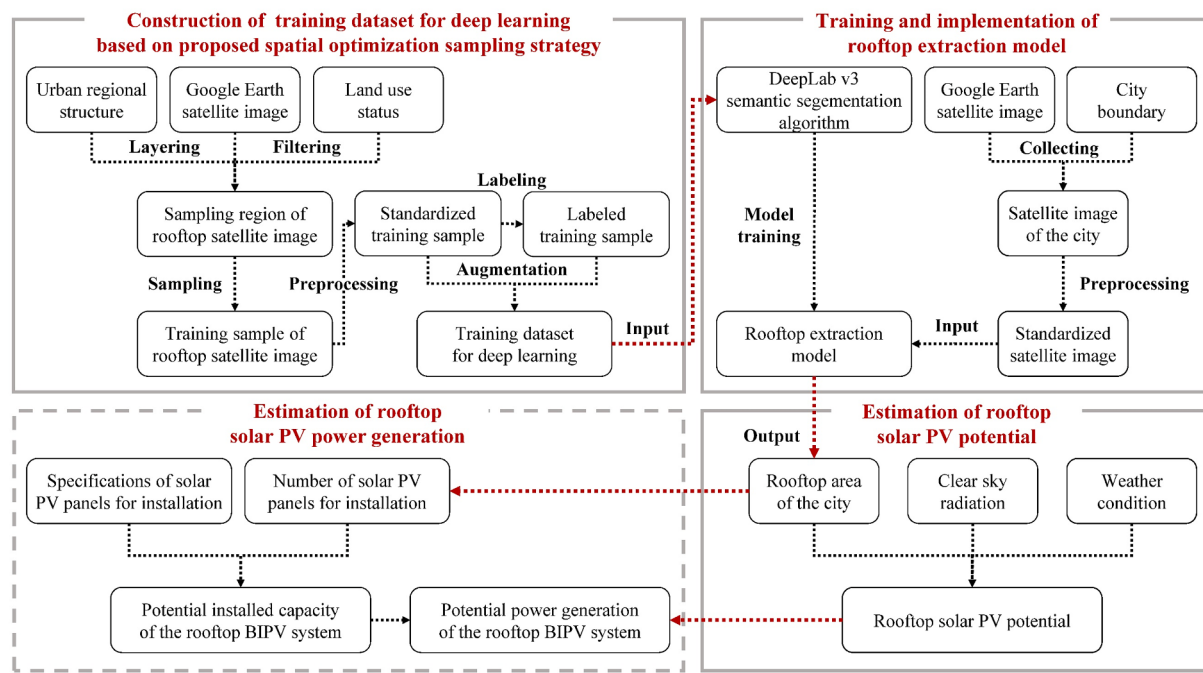


Fig. 1. Research flow chart.

[36]. Romero et al. used a high-accuracy 3D city model to calculate the total rooftop area and solar irradiance in Ludwigsburg, Germany [37]. Although a building's facade has a more available area than the rooftop, the building facade's solar PV potential is lower than that of rooftops [38]. Installing rooftop-mounted PV systems on urban buildings has great potential for reducing greenhouse gas emissions. A building's rooftop is considered a suitable place to install solar equipment without additional development [39]. In response to the current energy crisis and environmental degradation, rooftop solar PV integration effectively addresses the urban energy demand and environmental problems [30].

## 2.2. Acquisition of building rooftop information at the city scale

The rooftop area of buildings is the data basis for estimating the rooftop solar PV potential. However, currently, roof data cannot be obtained directly in most areas. Therefore, it is necessary to develop a city-scale acquisition method for building rooftop information.

### 2.2.1. Data sources for rooftop information acquisition for city buildings

High-resolution remote sensing data, including LiDAR and DSMs, have been widely used for extracting urban building rooftops. Jochem et al. used airborne laser scanning (ALS) data to detect all rooftop surfaces utilizing region growing [40]. Gooding et al. used model-driven methods to reconstruct a rooftop form from the low-resolution DSM [33]. However, these high-resolution remote sensing data are not affordable when applied at the city scale. Open-access data from public map service providers, including Google Earth and OpenStreetMap, have also been used for rooftop extraction. For example, Huang et al. used deep learning technology to extract rooftop areas based on GES images [16]. Public map services' public data have advantages in terms of extensive coverage, high update speed, and low acquisition cost. In particular, GES images with sub-meter-level resolution provide new opportunities for solar energy estimation at the city scale.

### 2.2.2. City-scale extraction method for building rooftop information

3D city models are usually constructed in advance to facilitate the extraction of building rooftops at the city scale. Agugiaro et al. used the Delaunay algorithm to construct a 3D city model based on LiDAR data [41]. The rooftop area can also be obtained with traditional edge

detection algorithms. Kabir et al. used object-based image analysis (OBIA) to extract rooftops from Quickbird satellite imagery [42]. This type of method usually uses low- or mid-level features to distinguish building objects from non-building objects. The results depend on the setting of certain thresholds or the use of decisive empirical rules [43]. As the study area continues to expand, the rooftop style tends to be diversified. As a result, the setting of thresholds or empirical rules will become more complicated, making it challenging to popularize such methods to be implemented at the city scale.

Recently, there has been an increase in the use of deep learning-based methods to extract rooftop information at the city scale. Mohajeri et al. proposed a support vector machine (SVM)-based method to classify rooftops into six categories according to the rooftop features [36]. Huang et al. obtained rooftop areas based on the image semantic segmentation model [16]. Semantic features have been widely used in the extraction of urban objects such as buildings, roads, and trees from satellite images [43]. For deep learning-based methods, a large training data set helps improve model performance. However, the additional amount of training data will increase data labeling's labor cost and the time cost of model training. When faced with a wide range of application scenarios, a way to maximize the efficiency of data input and performance output should be found instead of increasing the amount of data unscientifically.

In summary, the current research on the estimation of rooftop solar PV potential on a city scale is challenging to consider both the accuracy of the estimation results and the economic and time costs of large-scale application and promotion methods. The accuracy of rooftop extraction using the 3D building model method is relatively high, while the demanding specific remote sensing data products (e.g., 3D LiDAR data) are not affordable. Traditional image processing algorithms or spatial analysis algorithms need to manually determine the threshold value for image segmentation, which is challenging to be applied on a large-scale urban scale. In recent years, the image semantic segmentation algorithm based on deep learning enables the extraction of building rooftops on a city scale. However, the existing methods of extracting building rooftops from high-precision remote sensing images using deep learning have limitations in implementation cost. Especially the manually labeling of massive rooftop image samples for training the deep learning-based models is labor-intensive. In addition, the random sampling method of

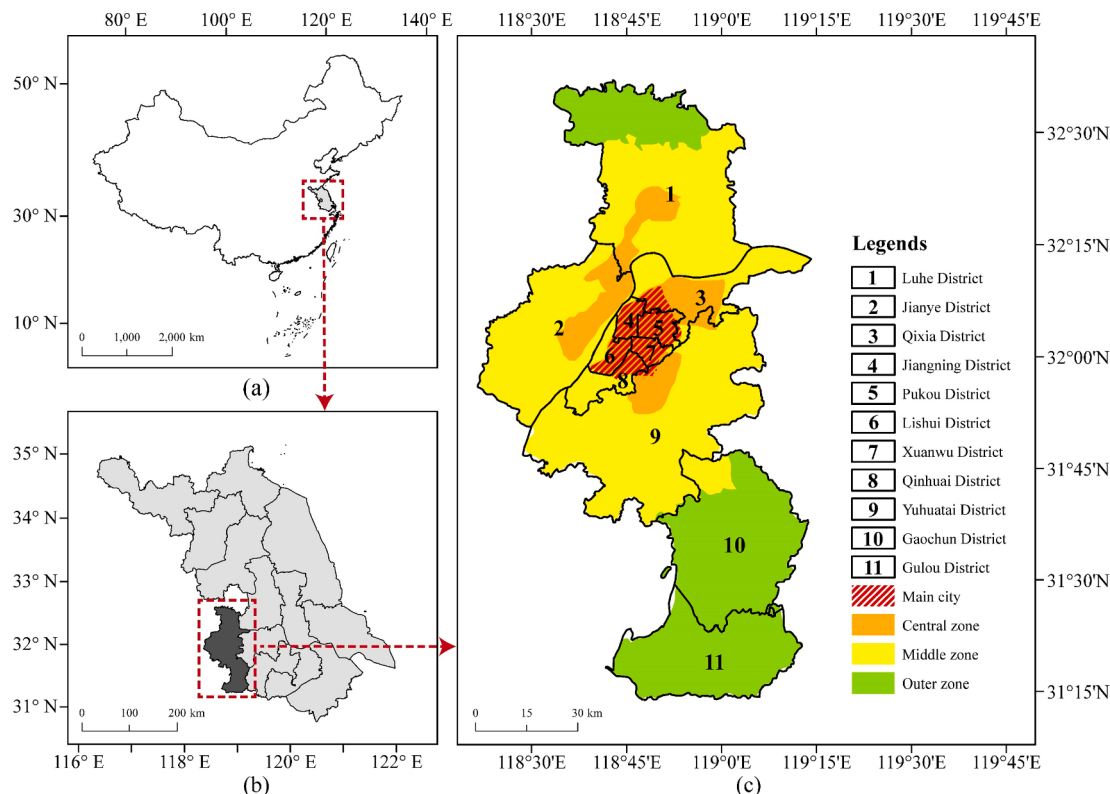


Fig. 2. Study area. (a) China, (b) Jiangsu Province, (c) Nanjing City.

sample images will lead to redundancy in the training dataset.

This study proposes a city-scale framework for the estimation of rooftop solar PV potential. Specifically, a novel training data acquisition strategy based on prior knowledge is developed to improve the proposed framework's feasibility when applied on a large scale. The estimated rooftop solar PV potential with this affordable framework can further support the estimation of rooftop solar PV power generation.

### 3. Methodology and research framework

To facilitate the elaboration of the method, Nanjing, China, was taken as the study area. Sample data were obtained based on GES images with prior knowledge of the study area. An image semantic segmentation model was designed to extract the image's rooftop part to support building-scale solar PV potential estimation.

In Section 3.1, the overall framework of the study is described. In Section 3.2, to avoid blindly increasing the amount of data, a spatial optimization sampling strategy using prior knowledge is proposed to obtain rooftop samples with good richness and balance. The construction of a training dataset for deep learning is further explained. In Section 3.3, the rooftop extraction technique based on deep learning used to achieve the city-scale acquisition of rooftop information is discussed. In Section 3.4, the extracted city-scale rooftop is applied to estimate the rooftop solar PV potential. In addition, the potential installed capacity and the corresponding potential annual power generation of the rooftop-mounted PV system are estimated based on the extracted city-scale rooftop.

#### 3.1. Overall research framework

The research framework consists of the following three main modules: the construction of a training dataset for deep learning based on the proposed spatial optimization sampling strategy, the training and implementation of the rooftop extraction model, and the estimation of

rooftop solar PV potential. The overall work framework and process, shown in Fig. 1, are as follows. In constructing a training dataset for deep learning, a spatial optimization sampling strategy was formulated, combined with prior knowledge about the urban and rural spatial structure and land use. A series of citywide satellite images were obtained as samples by stratified sampling. The collected samples were standardized and labeled, and data augmentation was performed to construct a training data set suitable for deep learning. The constructed dataset was input into the deep learning network for training in the rooftop extraction model's training and implementation. An image semantic segmentation model that extracts the rooftop in GES images could then be obtained. The rooftop area was then obtained by applying this model to the whole study area. The rooftop solar PV potential can be estimated based on the extracted rooftop. The proposed framework can also be applied to estimate the potential installed capacity and the corresponding potential annual power generation of the rooftop-mounted PV system.

#### 3.2. Construction of training dataset for deep learning based on proposed spatial optimization sampling strategy

##### 3.2.1. Study area

The study was conducted in Nanjing, Jiangsu Province, China (Fig. 2). Nanjing is the capital of Jiangsu Province and one of China's most historic cities with a resident population of 8.44 million by the end of 2018 and covers an area of 6587.02 km<sup>2</sup> [44]. The city has a subtropical monsoon climate with four distinct seasons. The annual precipitation is 1200 mm, and the annual average temperature is 15.4 °C [45]. Nanjing is the central city of the Nanjing Metropolitan Area that was jointly built by Jiangsu and Anhui provinces. With the continuous expansion of Nanjing's economy and population, the demand for energy consumption increases rapidly. In recent years, the energy transition in Nanjing has been improving energy efficiency to expanding the use of green energy (e.g., solar energy). Nanjing has favorable natural

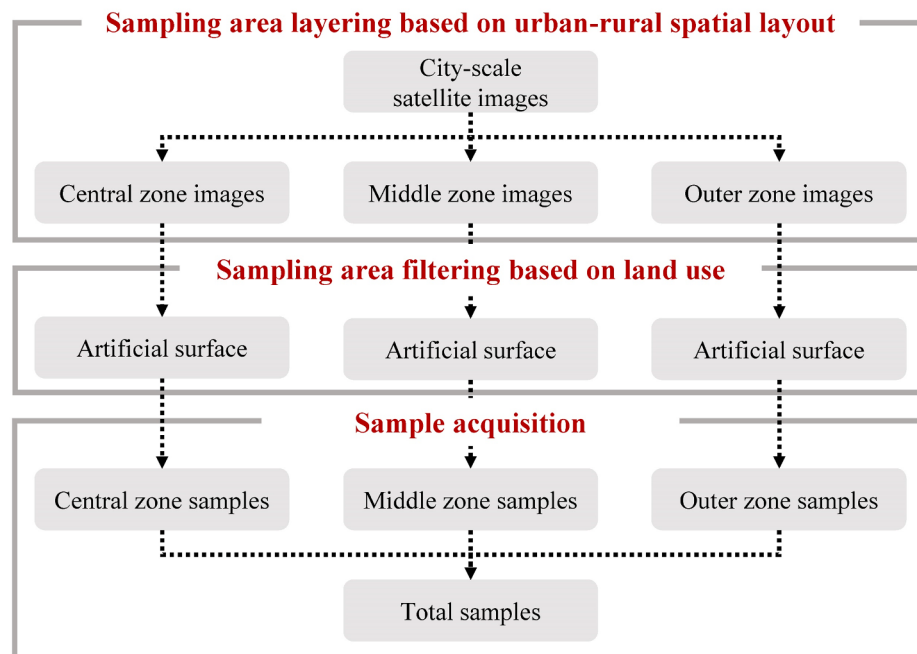


**Fig. 3.** Sampling process based on the layering and filtering strategy.

conditions for utilizing solar energy to generate electricity. There are many rooftops of residential buildings and factories in urban and rural areas of Nanjing that can significantly support the construction of rooftop solar PV projects. The study on Nanjing is of significance for implementing and promoting distributed rooftop solar PV projects in other metropolitan areas of China.

Nanjing includes 11 districts (Fig. 2c, black-bordered areas), three zones (Fig. 2c, orange, yellow and green areas), and the main city

(Fig. 2c, the area with red slashes). Typical verification areas were selected in each district to verify the accuracy of the rooftop extraction results. Nanjing, with 11 districts, is divided into three zones, the central zone (urban area), middle zone (urban-rural transitional area), and outer zone (rural area), according to the urban and rural spatial layout of Nanjing. The proportion of rooftop samples of different styles can be more balanced by setting a reasonable sampling amount in each zone. The main city is densely built with the highest level of construction in

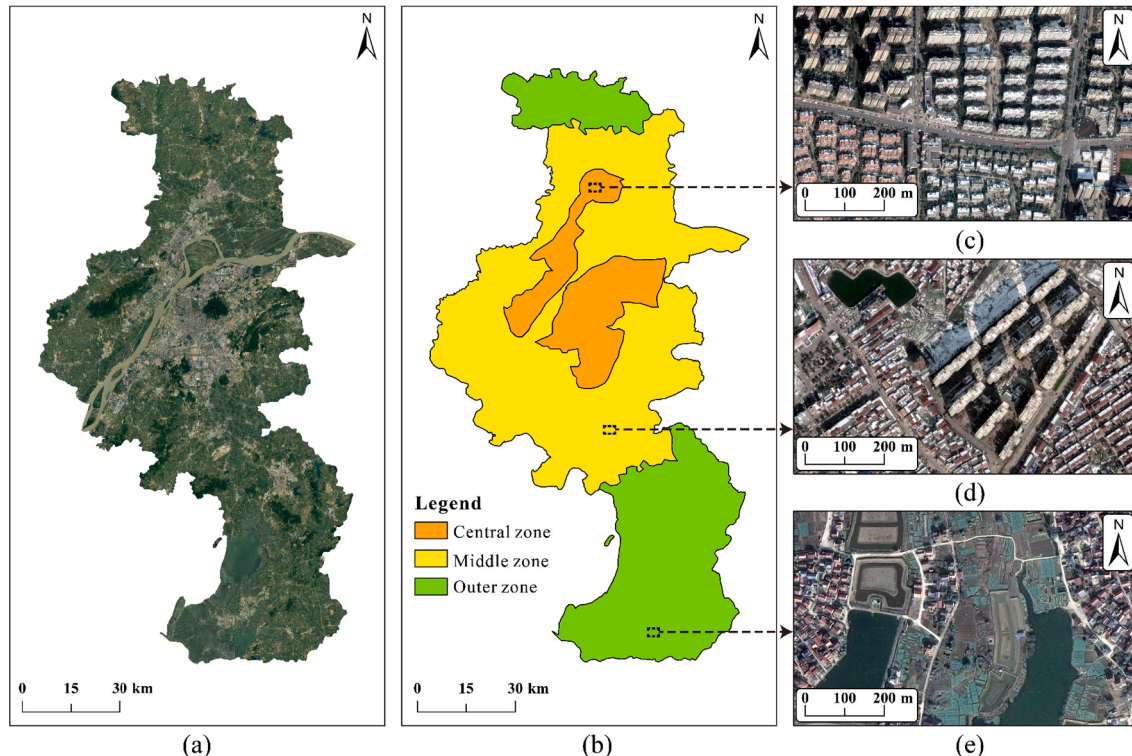


**Fig. 4.** Sampling area layering based on the urban and rural spatial layout. (a) GES image in Nanjing, (b) Division of urban and rural spatial layout in Nanjing, (c) Part of the central zone image, (d) Part of the middle zone image, (e) Part of the outer zone image.

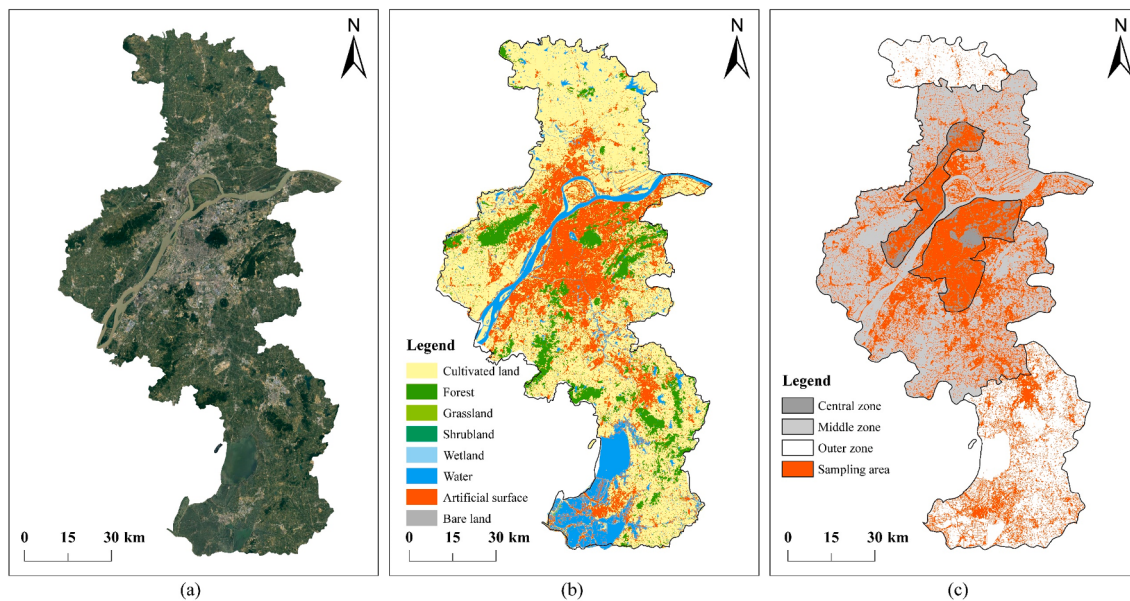


**Fig. 5.** Sampling area filtering based on the current situation of urban land use. (a) GES image in Nanjing, (b) Land use in Nanjing, (c) Sampling area in three zones.

Nanjing. Therefore, in Section 4, the main city was taken as an example further to demonstrate the estimated results of rooftop solar PV potential.

### 3.2.2. Citywide satellite image acquisition

This study used publicly available GES images as the data source. GES images have advantages in terms of accuracy and extensive coverage. According to the boundary vector data of Nanjing City, GES images within the Nanjing area were downloaded with Python scripts based on the open map service application program interface (Google Earth API) provided by Google. The image resolution of the downloaded GES images is approximately 0.25 m/pixel. Under this resolution, the details of a building can be displayed clearly.

### 3.2.3. Image layering and filtering based on prior knowledge

For deep learning, the model performance on vision tasks improves logarithmically as the magnitude of the training data increases. However, the data set should be organized with some prior knowledge instead of being increased arbitrarily. Under the same sample size, a well-organized data set with distinct characteristics improve the rooftop extraction model's performance. From the perspective of data acquisition, the spatial distribution and number of samples were determined in combination with Nanjing's urban morphology. The flowchart of the sampling process is illustrated in Fig. 3. First, the sampling area was layered into three parts, the central zone, middle zone, and outer zone, according to the urban and rural spatial layout. In each part, the sampling areas were selected, and only the artificial surface (a land use type refers to the surface formed by artificial construction activities, including residential areas, industrial and mining areas, and transportation facilities) was retained based on the land use of Nanjing. Finally, by adopting the spatial optimization sampling strategy based on prior knowledge, more abundant and distinctive rooftop samples were obtained in Nanjing.

#### A. Sampling area layering based on the urban-rural spatial layout

China's rapid urbanization has led to differing architectural characteristics between rural and urban residential buildings [46]. To make the rooftop extraction model more suitable for extracting rooftops of different styles in Nanjing, urban and rural architectural samples must be obtained as the training samples in a balanced manner. According to

**Table 1**  
Acquisition of the training samples based on prior knowledge.

Layering of sampling area	Layering result	Area (km <sup>2</sup> )	Proportion of each zone (%)
Central zone	867.10	13.16	
Middle zone	3524.85	53.50	
Outer zone	2196.39	33.34	
Total	6588.34	100.00	
Filtering of sampling area	Filtering result	Area (km <sup>2</sup> )	Artificial surface coverage of each zone (%)
Artificial surface of central zone	509.35	58.74	
Artificial surface of middle zone	669.73	19.00	
Artificial surface of outer zone	289.97	13.20	
Total	1469.05	22.30	

the Nanjing Urban Construction Plan, the urban-rural spatial layout in Nanjing's urban construction adopts the circular structure of the central city, metropolitan area, and city area [47]. The central urban area includes the main built-up area of the city. The municipality includes the central city and relevant scattered groups or satellite towns outside downtown. Between the metropolitan area and the city's administrative boundaries are generally small towns and the countryside in a large area far from the city center. According to the circular structure, the GES image of Nanjing (Fig. 4a) has been layered into three zones: the central zone, the middle zone, and the outer zone (Fig. 4b). Enterprises mostly lead the construction of buildings in the central zone, and the architectural style follows a unified standard (Fig. 4c). Individuals normally build the buildings in the outer zone, so the locations and styles have great randomness and subjectivity (Fig. 4e). The middle zone is the transition zone between the urban style and rural style (Fig. 4d).

#### B. Sampling area filtering based on land use

The study area (Fig. 5a) contains many areas, such as water surfaces and cultivated land, and the proportion of these non-target samples is much greater than that of our target samples (rooftops). Therefore, the samples must be further filtered and combined with information on

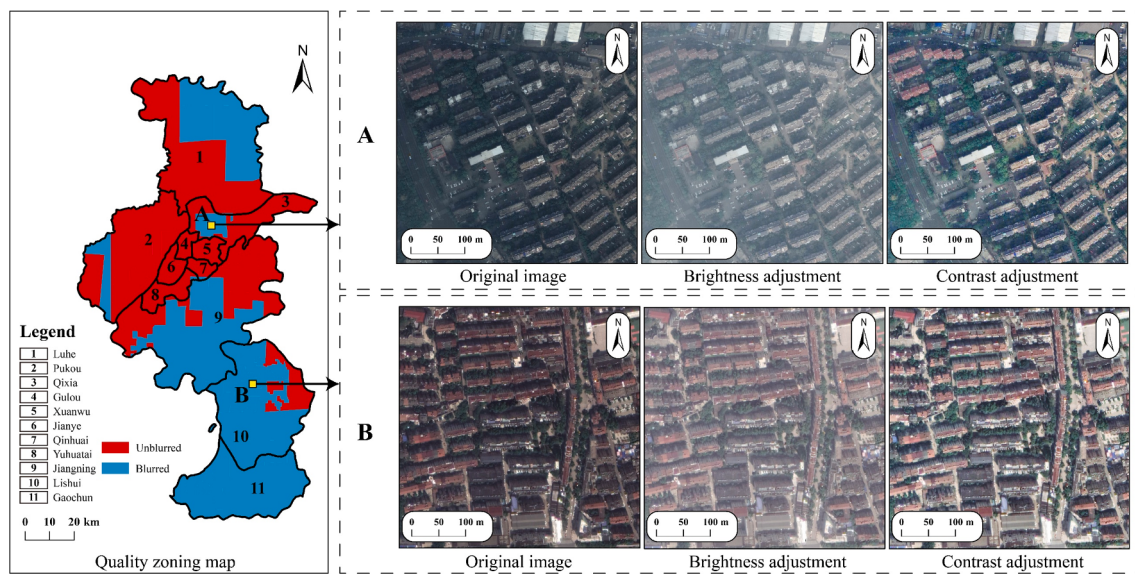


**Fig. 6.** Comparison of remote sensing images before and after pre-processing.

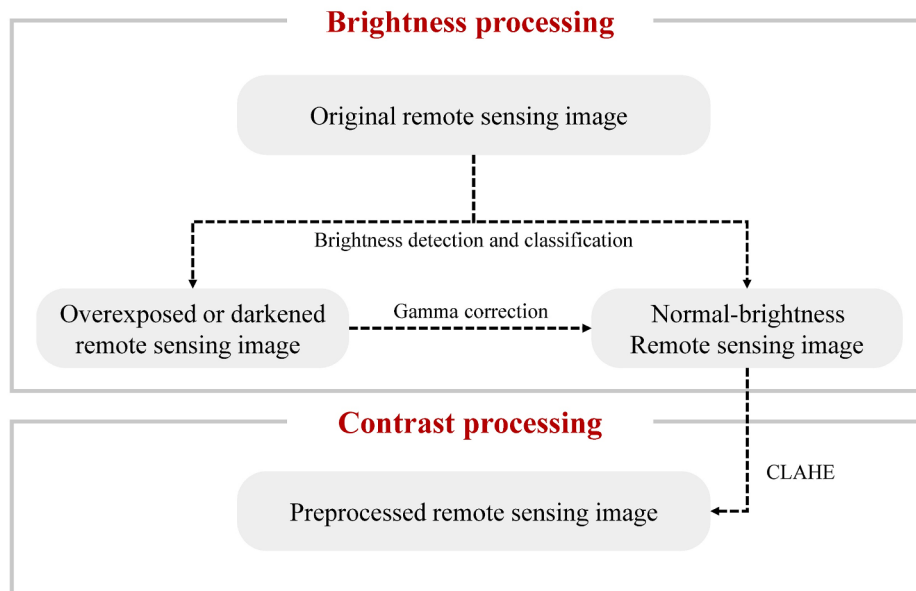


**Fig. 7.** Data pre-processing.

urban land use. The land use data were derived from the global 30-m surface coverage data (Globeland30) (Fig. 5b).<sup>2</sup> Artificial land surface categories were selected (Fig. 5c, red), and the scope of the sampling area was limited to this category.

#### 3.2.4. Sample acquisition

By layering the sampling area according to the urban and rural spatial layout and filtering the sampling area according to the current land use, a sample acquisition method based on a priori knowledge is proposed. As shown in Table 1, the central zone is small but has a high artificial surface coverage rate. In contrast, the middle zone is large but has a lower rate of artificial surface coverage. If the random sampling method is applied to collect the samples, there are many sample images with a small artificial surface. Besides, the buildings in the outer zone

have a rural-style rooftop. Random sampling will not be able to obtain enough samples of the rural style of rooftops. Therefore, to obtain enough sample images of rooftops in different styles, a sample acquisition strategy method based on a priori knowledge is needed.

In this study, the central zone, middle zone, and outer zone images were observed and studied. Based on the buildings' style characteristics in different zones and the proportion of visual observations, the assumption was made that the proportions of urban-style and rural-style buildings in the central and outer zones are the opposite. In contrast, the percentages in the middle zone are equal. Based on this assumption, the sample proportion was set in each partition. Based on this sample proportion, training samples were obtained from GES images throughout Nanjing with a Python script. To determine the appropriate sampling amount, we set up a series of different sampling amounts to prepare for the benefit curve's subsequent drawing.

<sup>2</sup> See <http://www.globallandcover.com>.

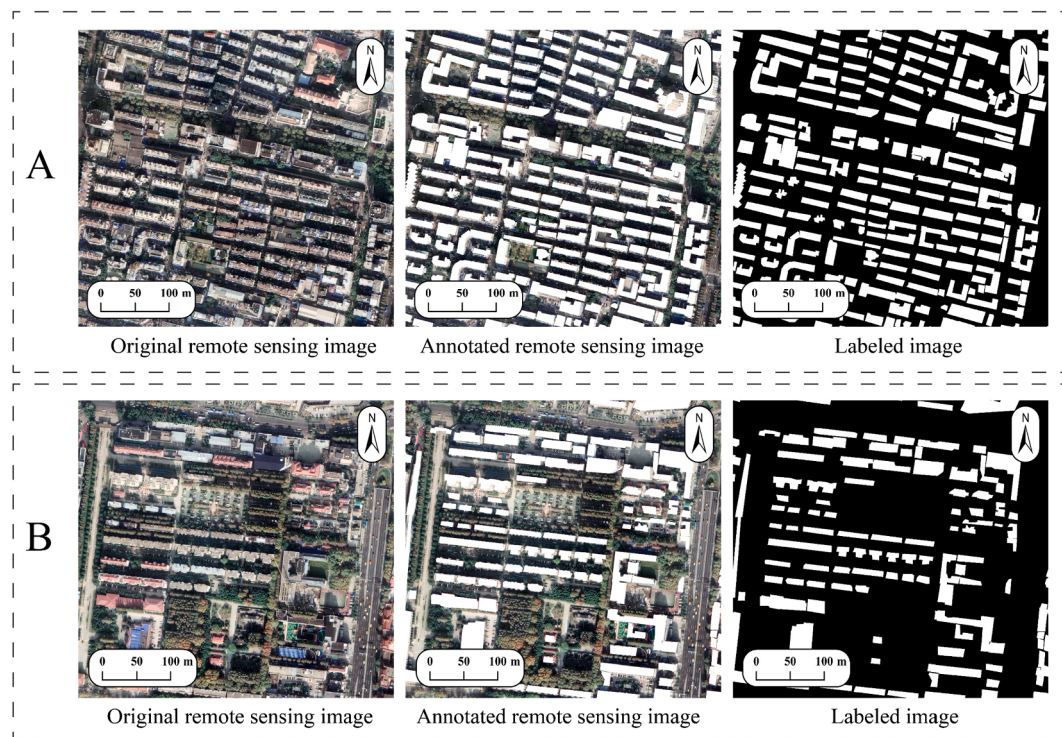


**Fig. 8.** Example of labeled image production results.

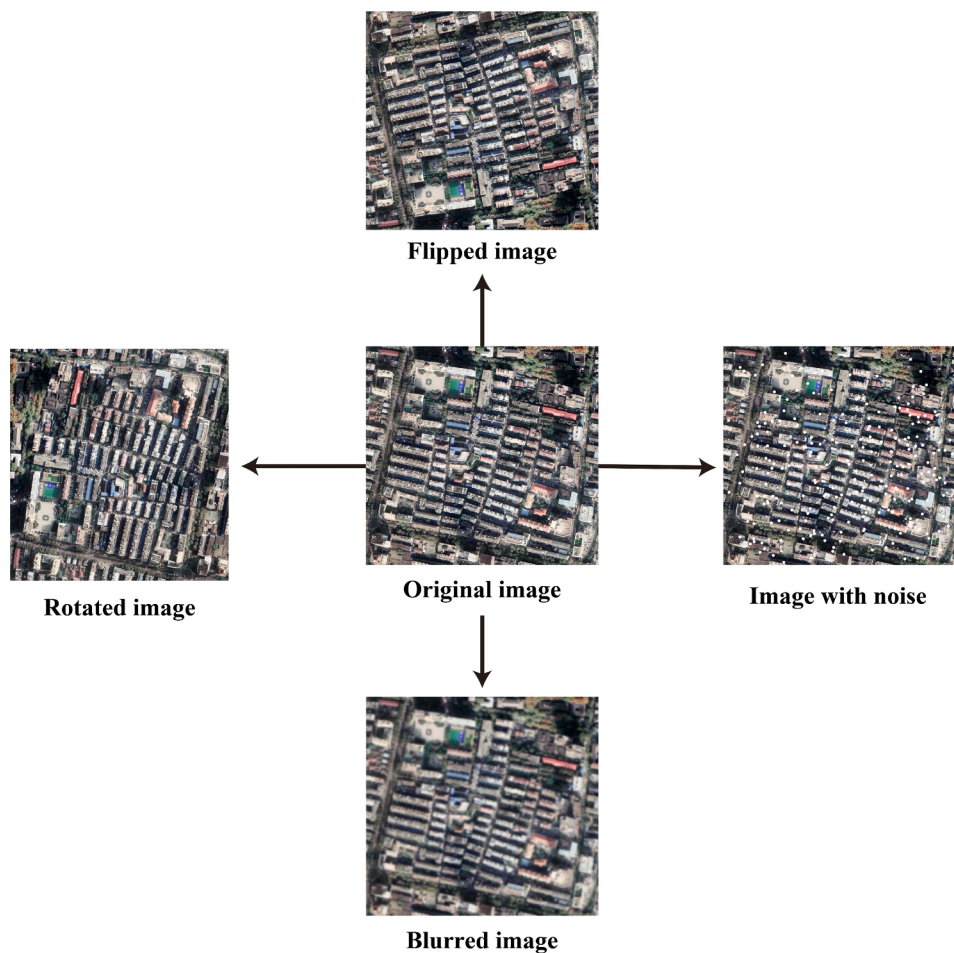


**Fig. 9.** Application example of the data augmentation method.

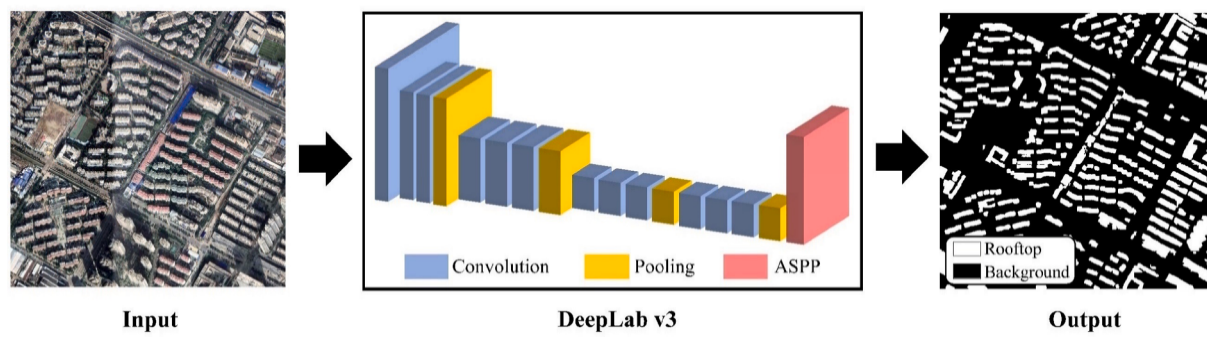


**Fig. 10.** Using a deep learning approach for rooftop segmentation.

### 3.2.5. Training sample standardization

A GES image's quality varies with the imaging system, imaging time, and environmental factors such as the atmosphere and climate (Fig. 6). A difference in image quality will add much interference information in the training and testing of the model. Therefore, these GES images must be pre-processed to improve their quality. In this study, brightness and sharpness are the two major quality problems of remote sensing images in the Nanjing area. Consequently, brightness processing and sharpness processing must be performed. The overall method of pre-processing is shown in Fig. 7.

In the brightness processing step, the input remote sensing image's brightness was detected to determine whether the image had normal brightness. A remote sensing image with an abnormal brightness level (such as an image that was overexposed or too dark) was adjusted with gamma correction. In the sharpness processing step, contrast limited adaptive histogram equalization (CLAHE) was conducted on the remote sensing image. Histogram equalization is essentially a non-linear stretching of the image. The image pixel values are redistributed so that the numbers of pixel values within a specific grey range are approximately equal. A comparison of images before and after remote sensing image pre-processing is shown in Fig. 6.

### 3.2.6. Sample labeling and augmentation

In this study's deep learning-method, a labeled image corresponding to a remote sensing image sample must be produced to carry out model training and testing. ArcGIS was used to mark the remote sensing image samples manually. A drawing tool was used to mark the rooftops in the remote sensing image samples one by one. An example of a labeled image production result is shown in Fig. 8.

Data augmentation is implemented to obtain sufficient data for training deep networks [48,49]. The remote sensing image samples were randomly processed for data augmentation. The data augmentation methods used included image rotation, image flipping, image blurring, and noise addition. In particular, adding noise to the training data can enhance the robustness of the model. Therefore, better performance can be achieved when images of low quality are input into the model. When the remote sensing image sample data were expanded, the labeled images corresponding to the sample were copied. An application example of the data augmentation method is shown in Fig. 9.

The training data set built in this study consisted of remote sensing image samples and corresponding labeled images after data pre-processing and data augmentation. There were a total of 20,000 remote sensing images in the sample, and the image size was  $256 \times 256$  pixels. Correspondingly, the labeled images totaled 20,000, and their size was  $256 \times 256$  pixels.

## 3.3. Training and implementation of rooftop extraction model

### 3.3.1. Rooftop extraction algorithm

Rooftops in Nanjing were extracted based on the image semantic segmentation algorithm DeepLab v3 using GES images. After the GES

images of Nanjing were acquired, rooftop image samples of typical areas were collected. The rooftop sample data were labeled before being entered into the DeepLab v3 algorithm to train the image semantic segmentation model suitable for city-scale rooftop extraction in Nanjing. DeepLab v3 is the latest version of the DeepLab series of open-source image semantic segmentation algorithms launched by the Google R&D team. The basic structure of DeepLab v3 is shown in Fig. 10. The blue region in the figure is the convolution layer, and the features extracted by each convolution kernel are different. The yellow region is the pooling layer. It takes the previous layer's feature map as input and samples the feature map to reduce the convolutional network's computational cost. The red region is atrous spatial pyramid pooling (ASPP). DeepLab v3 strengthens the extraction and differentiation of semantic information at different scales to achieve the segmentation of multi-scale objects in the target image.

### 3.3.2. Rooftop extraction model training

After the study area's rooftop samples were labeled; they were input into the DeepLab v3 model as a training data set. When training deep learning networks, due to computer memory and video memory's physical limitations, the training model's input size was set to  $256 \times 256$  pixels to improve the training efficiency and save video memory space. Besides, to improve the training model's extraction performance, the gradient descent method was used to optimize the training model algorithm. The core idea of the deep learning-based method is to use unsupervised learning for each network layer. Only one layer of the network was trained at a time, and the training results were used as the input to the next layer. Finally, supervised information feedback was used to adjust all the layers' weights. This feedback adjustment is usually carried out through gradient descent. There are three methods of gradient descent: batch gradient descent (BGD), stochastic gradient descent (SGD), and mini-batch gradient descent (MBGD). In the training process for this study model, the small-batch gradient descent method was used. The specific idea is to use a part of the samples to update each parameter. This can significantly reduce the number of iterations required for convergence, and at the same time, the convergence result can be brought closer to the gradient descent effect.

### 3.3.3. Rooftop extraction model application

After the rooftop sample data set was input to DeepLab v3 for training, an ideal model suitable for Nanjing rooftop extraction was obtained. By inputting all the satellite images of Nanjing City to be classified into this model, the satellite images' rooftop portions could be identified. Since the input image size was  $256 \times 256$  pixels when training the Nanjing rooftop extraction model, the size of the input images for prediction should also be  $256 \times 256$  pixels. However, the size of the acquired high-precision satellite image of Nanjing was much larger than the input size specified in the prediction. Therefore, it was necessary to divide the satellite image of the entire city of Nanjing into blocks. The original satellite image was processed into multiple standard images after block processing. The numerous standard images were then

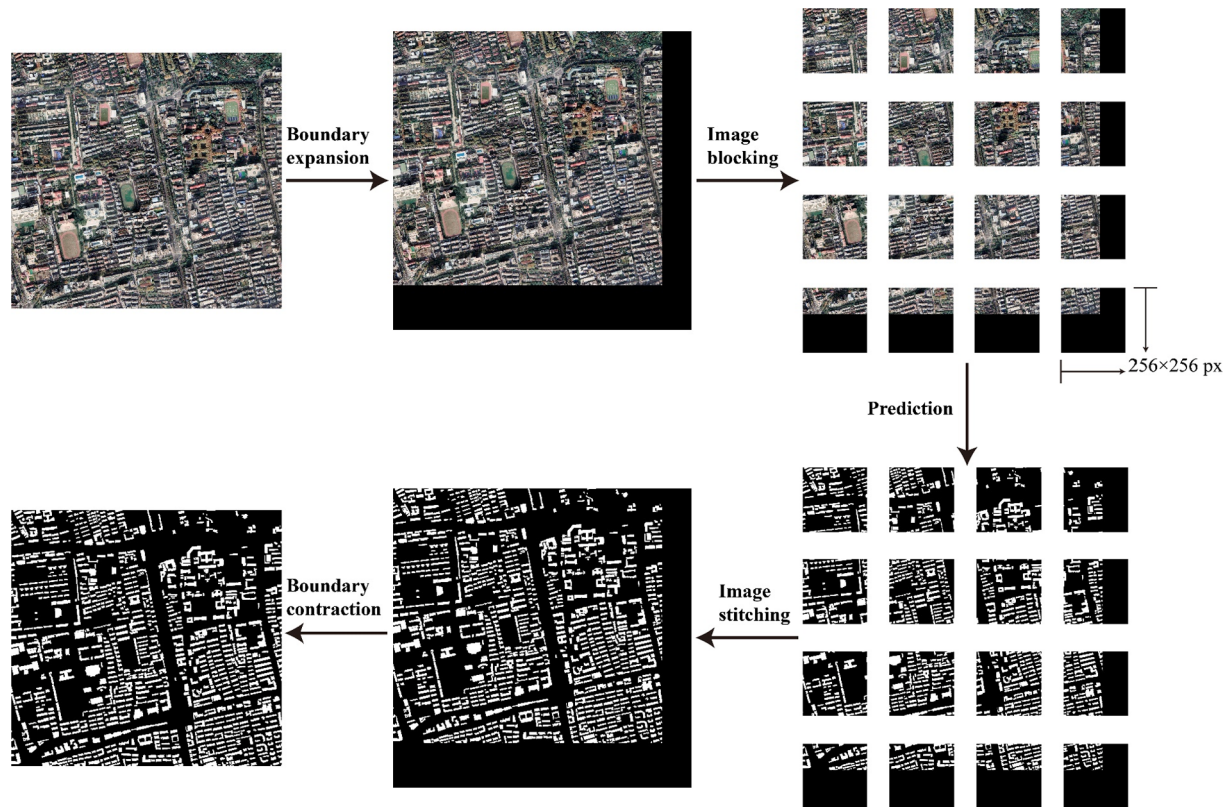


**Fig. 11.** Block prediction process.

inputted into the Nanjing rooftop extraction model for prediction. Finally, each block's prediction results were stitched together to complete the entire satellite image's prediction. The specific process is shown in Fig. 11. With this block prediction method, the trained rooftop extraction model could be applied to satellite images throughout Nanjing, and the rooftop image classification results for Nanjing were finally obtained.

### 3.3.4. Performance evaluation of the rooftop extraction model

#### A. Verification area

After the city-scale extraction of the rooftop features of Nanjing City through the DeepLab v3 model, the model's extraction performance needed to be verified. Four square kilometers of typical verification areas from densely constructed regions of 11 jurisdictions in Nanjing were selected and combined with Nanjing's administrative divisions' characteristics and the land use types in each administrative district. Verification areas with a total area of 44 km<sup>2</sup> were used for the performance assessment of the Nanjing rooftop extraction model. In terms of architectural style, both urban and rural architectural styles were considered. In terms of spatial distribution, the building features of 11 subordinate areas of Nanjing were selected. Therefore, the verification areas chosen in this study can objectively evaluate the Nanjing rooftop extraction model's overall performance.

#### B. Evaluation index

The confusion matrix and the four indicators calculated by the confusion matrix—accuracy, recall, precision, and comprehensive evaluation—were used to evaluate the performance of the Nanjing rooftop extraction model.

The confusion matrix is an error matrix used in machine learning to evaluate the model's performance. For a binary classification model, the

**Table 2**  
Definition of the confusion matrix.

Element	Definition
False Positives (FP)	Negative samples predicted as positive by the model
False Negatives (FN)	Positive samples predicted as negative by the model
True Positives (TP)	Positive samples predicted as positive by the model
True Negatives (TN)	Negative samples predicted as negative by the model

confusion matrix is a table with two rows and two columns composed of False Positives (FP), False Negatives (FN), True Positives (TP), and True Negatives (TN). The larger numbers of TP and TN and smaller numbers of FP and FN will indicate a better performance of the model. The specific definition of the confusion matrix is shown in Table 2. The confusion matrix counts the number of pixels, which leads to difficulties in measuring the pros and cons of the model with massive data. Therefore, the Accuracy, Precision, and Recall are calculated from a confusion matrix for a binary classifier. For the purpose of standardized

**Table 3**  
Definition of evaluation index.

Expression	Meaning
$Accuracy = \frac{TP + TN}{TP + TN + FP + FN}$	The ratio of the rooftop and background correctly extracted by the model to the total rooftop and background
$Precision = \frac{TP}{TP + FP}$	The ratio of the rooftop correctly extracted by the model to the total rooftop extraction, describing the precision of rooftop extraction result
$Recall = \frac{TP}{TP + FN}$	The ratio of the rooftop correctly extracted by the model to the actual total rooftop, describing the coverage of the rooftop extraction result
$F1 Score = \frac{2 \times Precision \times Recall}{Precision + Recall}$	A comprehensive evaluation of the recall and precision of rooftop extraction result

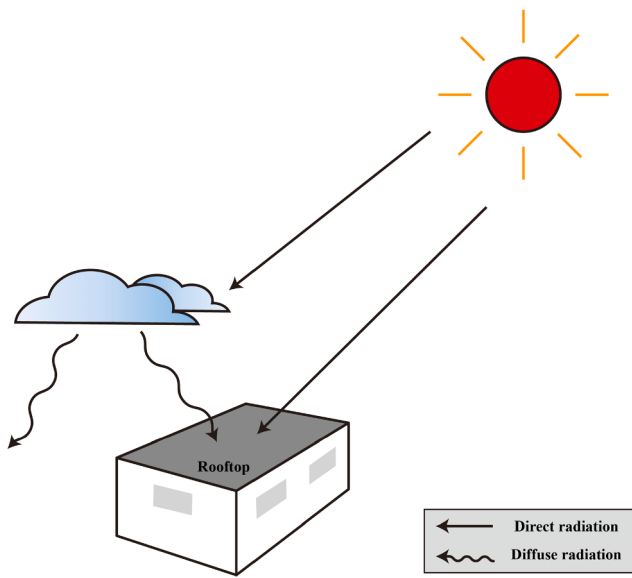


**Fig. 12.** Schematic diagram of the solar radiation received by a building rooftop.

measurement, the quantity in the confusion matrix will be transformed into a ratio between 0 and 1. The closer the value is to 1, the better the performance of the model. The F1 Score is a weighted average of Recall and Precision. Its value range is 0–1, the closer to 1 represents the better the model's performance. The specific definitions of accuracy, precision, recall, and comprehensive evaluation index F1 score are shown in Table 3.

#### 3.4. Estimation of rooftop solar PV potential

##### 3.4.1. Rooftop solar PV potential estimation model

The solar radiation data used in this study come from the Copernicus Atmosphere Monitoring Service (CAMS).<sup>3</sup> These data are solar radiation data at the surface level with a clear sky taken at hourly intervals, and they are publicly available free of charge. In this study, the rooftop of a building is regarded as a horizontal plane. Combined with clear sky radiation data ( $\text{Wh}/\text{m}^2$ ) and cloud cover correction parameters, the total amount of solar radiation received on the buildings' rooftop is estimated.

The total solar radiation reaching the ground consists of direct radiation and diffuse radiation [50], as shown in Fig. 12. The formula for calculating the total radiation at the surface level is as follows [51]:

$$\text{GHI} = \text{BHI} + \text{DHI} \quad (1)$$

where  $\text{GHI}$  is the global horizontal irradiance,  $\text{BHI}$  is the beam horizontal irradiation, and  $\text{DHI}$  is the diffuse horizontal irradiance.

The formula for calculating the true acceptable solar radiation in the horizontal plane is as follows [52]:

$$\text{GHI}_r = \text{BHI}_h \cdot M_t + \text{DHI}_h \cdot M_d \quad (2)$$

where  $\text{GHI}_r$  is the actual solar radiation received by the horizontal plane,  $\text{BHI}_h$  is the horizontal solar radiation under clear sky conditions,  $M_t$  is the monthly atmospheric transmittance,  $\text{DHI}_h$  is the horizontal solar radiation under clear sky conditions, and  $M_d$  is the monthly diffusion ratio.

The formulas for calculating the monthly atmospheric transmissivity ( $M_t$ ) and diffuse proportion ( $M_d$ ) from cloud data are as follows [52]:

**Table 4**

Summary of the weather condition in Nanjing in each month of 2019.

Month	Sunny days	Cloudy days	Total days	$P_{clear}$	$P_{cloudy}$
January	16	15	31	51.61%	48.39%
February	9	19	28	32.14%	67.86%
March	20	11	31	64.52%	35.48%
April	15	15	30	50.00%	50.00%
May	23	8	31	74.19%	25.81%
June	19	11	30	63.33%	36.67%
July	10	21	31	32.26%	67.74%
August	9	22	31	29.03%	70.97%
September	18	12	30	60.00%	40.00%
October	23	8	31	74.19%	25.81%
November	23	7	30	76.67%	23.33%
December	20	11	31	64.52%	35.48%

$$M_t = 0.7 \cdot P_{clear} + 0.3 \cdot P_{cloudy} \quad (3)$$

$$M_d = 0.2 \cdot P_{clear} + 0.7 \cdot P_{cloudy} \quad (4)$$

where  $P_{clear}$  is the proportion of sunny days in a month, and  $P_{cloudy}$  is the proportion of cloudy days in a month. We use World Weather Online to obtain the sunny and cloudy days in each month to determine  $P_{clear}$  and  $P_{cloudy}$ .<sup>4</sup> We have given specific values in Table 4.

The annual solar radiation (ASR) of all rooftop surfaces in the study area is estimated as follows:

$$\text{ASR} = \sum_{i=1}^{n_1} \left( \sum_{m=1}^{12} \left( \sum_{h=0}^{23} \left( \sum_{d=1}^{n_2} (S_i \times \text{GHI}_{rmdh}) \right) \right) \right) \quad (5)$$

where  $S_i$  represents the area of the  $i^{\text{th}}$  rooftop, and  $\text{GHI}_{rmdh}$  represents the corrected real solar radiation between the times  $h$  and  $h+1$  in the  $m^{\text{th}}$  month on the  $d^{\text{th}}$  day of the year.  $i$  represents the number of a rooftop ( $i = 1, 2, 3, \dots, n_1$ ), and  $n_1$  represents the total number of rooftops.  $m$  represents the month ( $m = 1, 2, 3, \dots, 12$ ).  $h$  represents the time in the 24-hour system ( $h = 0, 1, 2, \dots, 23$ ). The actual duration of received radiation is from sunrise to sunset on each day.  $d$  represents the day of the month ( $d = 1, 2, 3, \dots, n_2$ ), and  $n_2$  represents the actual number of days per month.

The model's input data are the hourly solar radiation data, monthly atmospheric transmittance, diffusion ratio, and rooftop surface (stored in the ESRI shapefile format). The simulation time interval is 1 h. The radiation estimation results for different periods can be generated according to the research design. This study shows the total annual acceptable solar radiation and the monthly total solar radiation per hour are obtained.

##### 3.4.2. Performance evaluation of rooftop solar PV potential estimation model

In this study, the initial input solar irradiance was calculated under the clear sky's assumption with the very pure clearness. There is still a need to estimate the received solar irradiation under the influence of real-world weather conditions. We use the formula (3) and (4) in Section 3.4.1 to correct weather conditions' negative influence. The best approach to validate our model's results is to use ground-truth data from either pyranometers solar radiation measuring equipment or installed solar PV systems [53]. Before obtaining the ground truth data, the observed solar radiation values of standardized weather stations are used for verification to obtain a certain understanding of the rooftop solar PV potential estimation results' overall accuracy.

The observed solar radiation data set can be obtained from the China Meteorological Administration, which includes the monthly average

<sup>3</sup> See <http://www.soda-pro.com/web-services/radiation/cams-radiation-service>.

<sup>4</sup> See <https://www.worldweatheronline.com>.

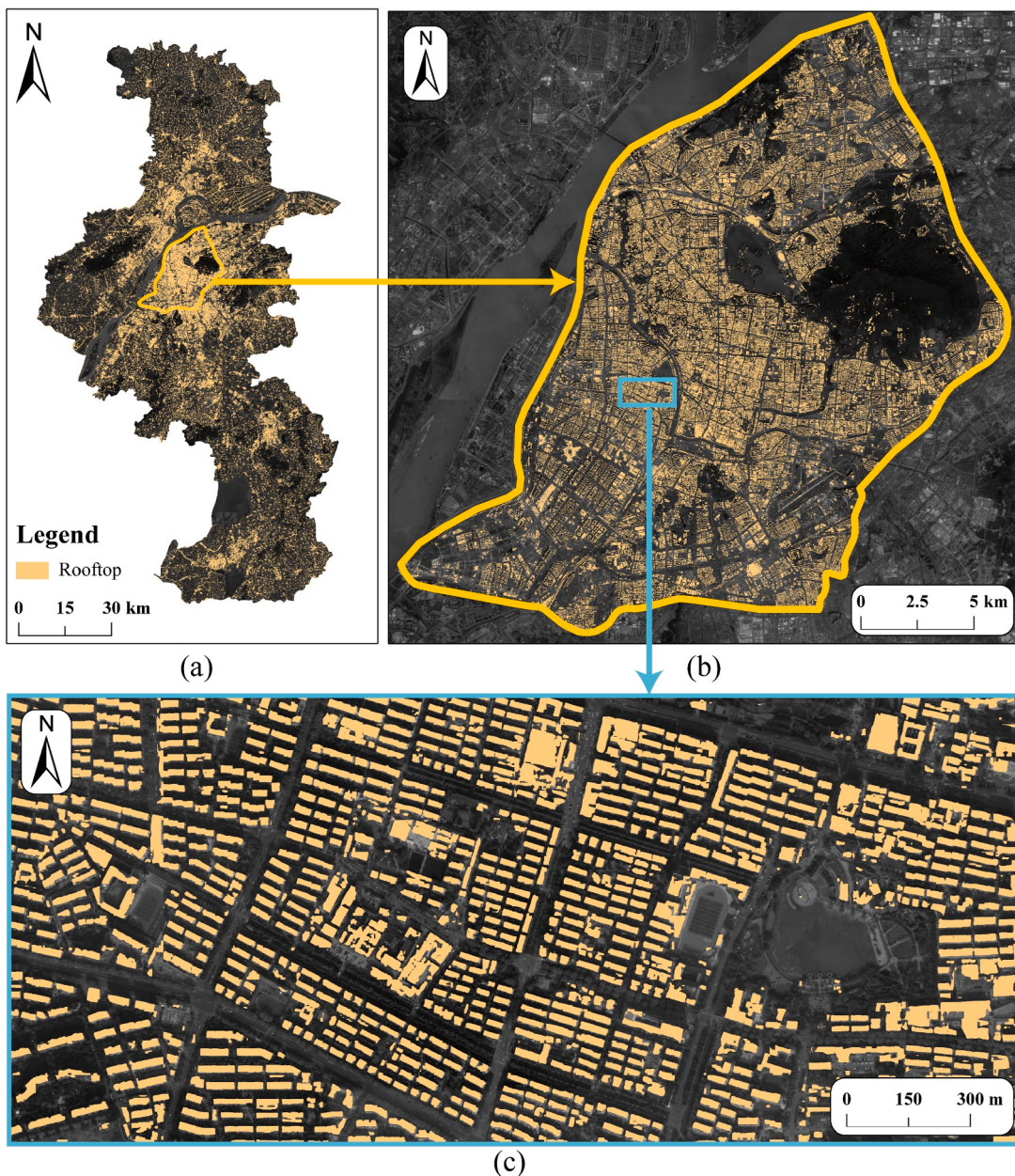


**Fig. 13.** Results of rooftop extraction. (a) Results of rooftop extraction in Nanjing, (b) Results of rooftop extraction in the main city of Nanjing, (c) Details of the rooftop extraction results in Nanjing.

solar radiation based on multi-year observation results, in kWh/m<sup>2</sup>/day.<sup>5</sup> The observed solar irradiance values were further used to compare with the corrected ones. The RMSE and Pearson product-moment correlation coefficient (Pearson's  $r$ ) were involved as the quantitative indicators to evaluate the proposed rooftop solar PV potential estimation model's performance. The RMSE measures the average difference between the corrected and the observed values, while Pearson's  $r$  measures the linear correlation between them. They are calculated as follows:

$$RMSE = \sqrt{\frac{\sum_{12}(G - G_{obs})^2}{12}} \quad (6)$$

$$r = \frac{\sum_{12}(G - \bar{G})(G_{obs} - \bar{G}_{obs})}{\sqrt{\sum_{12}(G - \bar{G})^2} \sqrt{\sum_{12}(G_{obs} - \bar{G}_{obs})^2}} \quad (7)$$

where  $G$  is the corrected daily solar irradiance,  $G_{obs}$  is the monthly mean daily solar irradiance observed in a meteorological station,  $\bar{G}$  and  $\bar{G}_{obs}$  are the mean values of the mean daily solar irradiance in the months of a year.

#### 4. Study results and discussion

In the previous section, the processes of sample acquisition, sample processing, rooftop extraction and estimation are illustrated. In this section, the results are described to demonstrate the performance of the proposed framework for the case study in Nanjing of both rooftop solar PV potential and rooftop solar PV power generation.

<sup>5</sup> See <http://data.cma.cn/>.

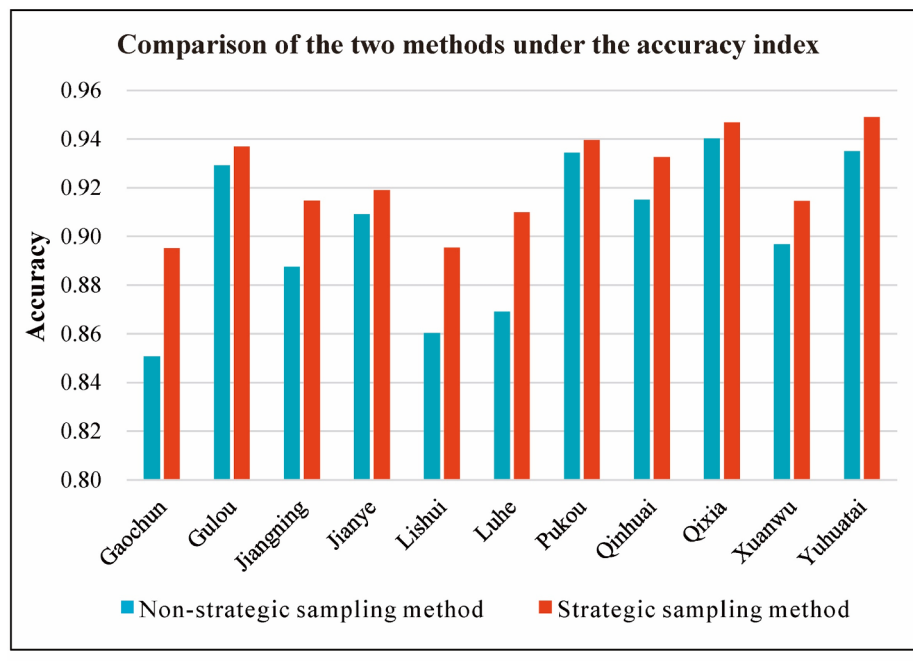
**Table 5**

Comparison of the model performance under strategic and non-strategic sampling methods in Nanjing.

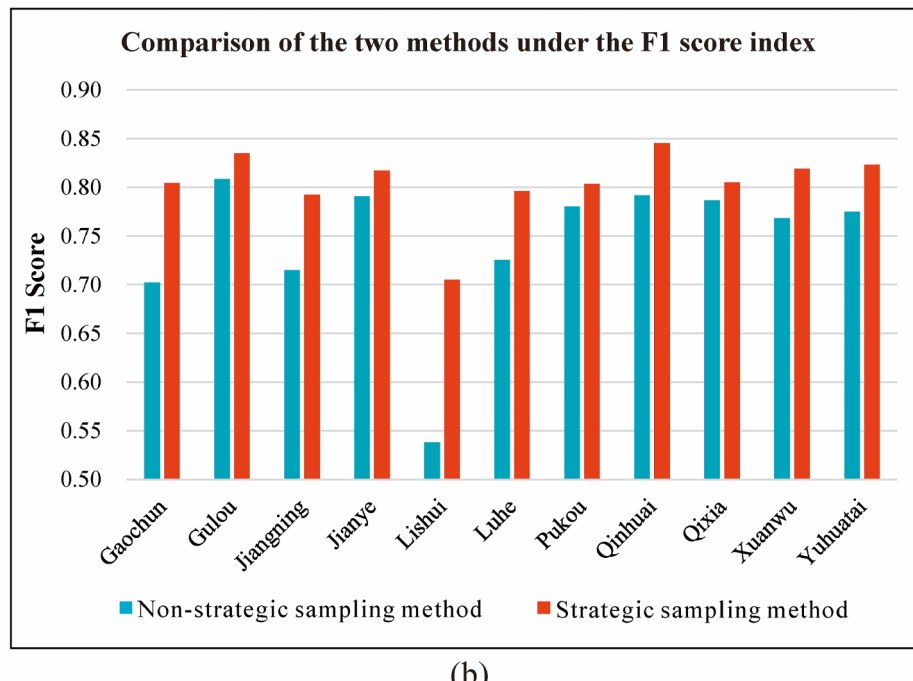
Method	Accuracy	Precision	Recall	F1-Score
Non-strategic sampling method	0.90	0.80	0.71	0.74
Strategic sampling method	0.92	0.82	0.79	0.80
Improvement	0.02	0.02	0.08	0.06

#### 4.1. Rooftop extraction results

In Nanjing, the total rooftop area is 330.36 km<sup>2</sup>. A more detailed rooftop extraction result is illustrated in Fig. 13(b) and (c). The rooftop extraction model's performance evaluation based on the strategic sampling method was conducted in 11 verification areas in Nanjing. The overall model performance evaluation of both the non-strategic sampling method and the strategic sampling method are summarized, and the results are shown in Table 5. Compared with the rooftop extraction model based on the non-strategic sampling method, the accuracy of the rooftop extraction model based on the strategic sampling method is improved by 2%, the precision value is improved by 2%, the recall value



(a)



(b)

**Fig. 14.** Comparison of the two methods under different indexes. (a) Comparison of the two methods under the accuracy index, (b) Comparison of the two methods under the F1 score index.

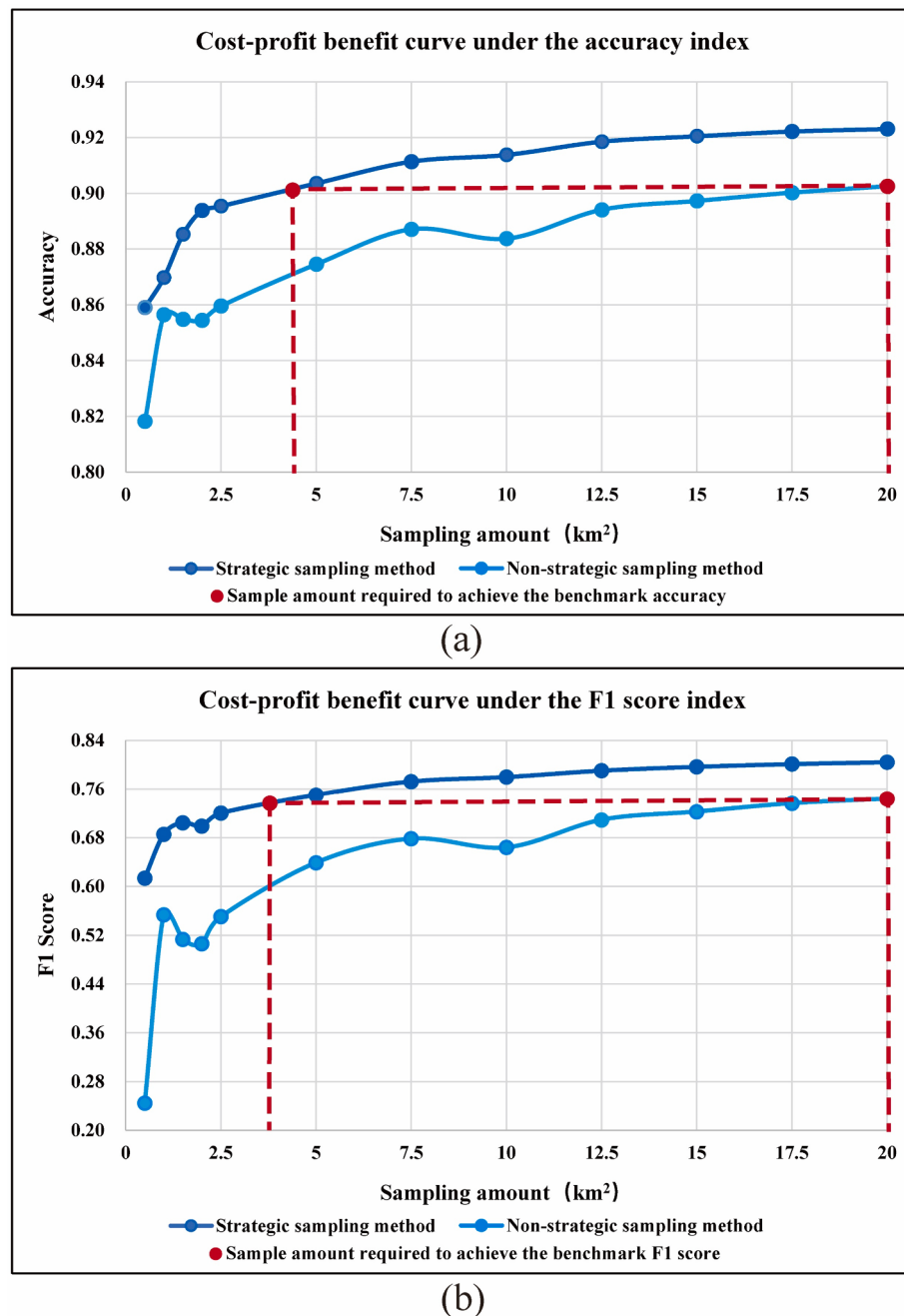


Fig. 15. Cost-profit benefit curve. (a) Cost-profit benefit curve under the accuracy index, (b) Cost-profit benefit curve under the F1 score index.

is increased by 8%, and the F1 score value is increased by 6%.

In this study, GES images were used to extract rooftop areas. GES image is not an orthorectified image, which leads to a position offset between the extracted rooftop contours and the ground truth. This position offset is more significant, which is about 20 m, at high-rise buildings, while it is insignificant for low-rise buildings. This position offset will not affect the accumulated rooftop areas for the city-scale rooftop solar PV potential estimation.

The extracted rooftop does not contain detailed structural information of the rooftop. Therefore, the extracted rooftop area is not identical to the usable rooftop area to install PV panels for real implementation. It is difficult to accurately extract the rooftop's geometric form, in terms of slope and aspect, based on the GES image. The reconstruction of the rooftop's detailed structural information relies on a high-precision 3D rooftop model that is difficult for the estimation on a city scale. Future

research will integrate methods for reconstructing rooftop geometry using publicly available street view images [54].

The proposed spatial optimization sampling strategy's contribution to constructing an efficient training dataset is mainly reflected in two aspects. On the one hand, the layering of the sampling areas improves the rooftop samples' style diversity. On the other hand, the filtering of sampling areas increases the abundance of rooftop samples and improves sampling efficiency. Therefore, in addition to the improvement in rooftop extraction's overall performance, the rooftop extraction model trained based on the strategic sampling method shows better robustness for rooftop extraction in each. Moreover, the training sample size required by the strategic sampling method is considerably smaller than that of the non-strategic sampling method when the rooftop extraction model is trained to achieve a target accuracy to satisfy the accuracy requirement.

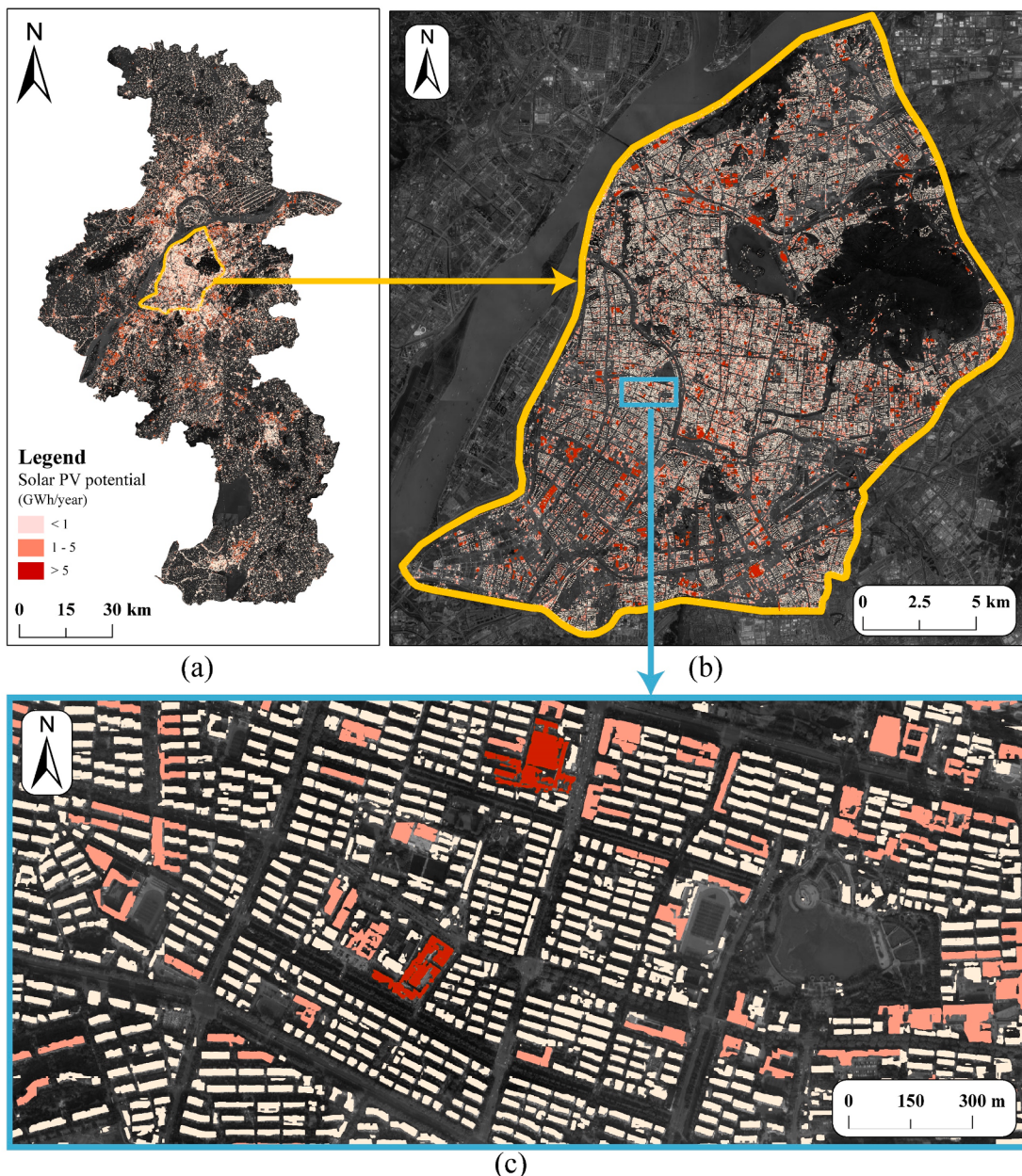


**Fig. 16.** Solar PV potential on rooftops. (a) Results of rooftop solar PV potential estimation in Nanjing, (b) Distribution of the estimated rooftop solar PV potential in the main city of Nanjing, (c) Details of the rooftop solar PV potential distribution in Nanjing.

The rooftop extraction model's performance was evaluated in each region to demonstrate further the robustness of the rooftop extraction model trained by image samples collected with the strategic sampling method. The evaluation results are shown in Fig. 14. If 0.88 is used as the threshold of the accuracy rate, the model evaluation results under the non-strategic sampling method do not meet the standard in Gaochun, Lishui, and Luhe. This is for two main reasons. The first is that these three verification areas are located on the outer edge of the city. The architectural style is mostly rural. The houses under this style generally occupy a small area. The site layouts have strong randomness and subjectivity. This increases the difficulty of accurate model identification. Furthermore, because the GES image's quality is inconsistent between regions and these three more remote verification areas are in areas where the image quality is degraded, this also causes difficulty in model identification to a certain extent.

However, through the strategic sampling method, a training data set with better richness and balance is constructed. The final model's

universality was improved to address the above identification difficulties caused by differences in the building distribution and building style. After the strategic sampling method is used, the accuracy of model identification is improved in each area. In particular, for areas with more rural-style buildings such as Gaochun, Lishui, and Liuhe, the recognition accuracy is notably enhanced. In the study area in Gaochun, with the lowest recognition accuracy of 0.85, the recognition accuracy of the current model is 0.90, so it has also been improved.

A comparative study of sampling amount and model performance is conducted to demonstrate further the study's strategic sampling method's beneficial influence. Fig. 15 shows the cost-profit benefit curve under the strategic sampling method and the non-strategic sampling method. In terms of the method promotion's cost input, the sampling amount required by the strategic sampling method is significantly smaller than that of the non-strategic sampling method when the model performance is equal. Taking the random sampling method's model performance in 20 km<sup>2</sup> as the benchmark, we use the red indicator line

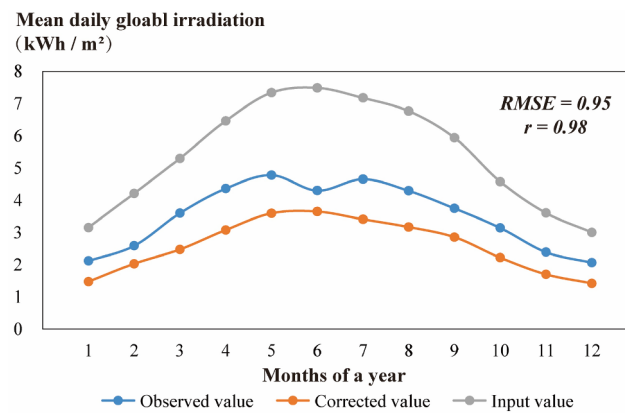


Fig. 17. Corrected results of monthly solar irradiation.

to show the difference in sampling amount between the two methods to achieve it. In strategic sampling, only approximately 20% of the sampling amount is required to achieve the benchmark accuracy, and the sampling amount input is reduced by about 80%. This shows that the sampling method based on prior knowledge can significantly reduce the cost of sampling and annotation, and a small number of samples can be collected for training to obtain a model that can be applied to rooftop extraction over the whole city.

#### 4.2. Estimation and temporal analysis of the rooftop solar PV potential

##### 4.2.1. Rooftop solar PV potential estimation results

The solar radiation that the city's rooftops can receive was estimated based on Nanjing's rooftop extraction results. The results are displayed according to a three-level scale (Fig. 16). Fig. 16(a) shows the rooftop solar PV potential in Nanjing City. Fig. 16(b) shows the distribution of the estimated rooftop solar PV potential in downtown Nanjing. Taking a small local area as an example, the details of the rooftop solar PV potential's estimation results are presented in Fig. 16(c).

According to our calculation results, the annual rooftop solar PV potential in Nanjing is 311,853 GWh. A certain number of the individual rooftops in Nanjing had an annual rooftop solar PV potential of more than 1 GWh as of 2019. rooftops with larger available areas can receive more solar radiation. The results show that there are some rooftops with solar PV potentials greater than 5 GWh distributed outside Nanjing's downtown. This is because large-scale industrial factory buildings with large rooftop areas moved to the suburbs during the industrial restructuring and upgrading in Nanjing.

The value of *RMSE* is always no less than 0, and a lower *RMSE* means better goodness of fit to the observation data. Pearson's *r* has a value between -1 and 1. The closer the Pearson's *r* is to 1, the better the

correction of weather condition is. Fig. 17 shows the input, corrected, and observed values of solar irradiation for each month in Nanjing. The input values (in gray) of monthly mean daily solar irradiance under the clear sky range from 3.01 (December) to 7.49 kWh/m<sup>2</sup> (June). The observed values (in blue) of monthly mean daily solar irradiance by a radiometer at the meteorological station range from 2.07 (December) to 4.78 kWh/m<sup>2</sup> (May). The real-world solar irradiance has been overestimated in different degrees.

Based on formula (3) and (4) in Section 3.4.1, the theoretical values of mean daily solar irradiance of the 12 months were corrected (in red). The corrected values in Nanjing range from 1.42 (December) to 3.65 kWh/m<sup>2</sup> (June). The corrected curve is closer to that of the observed values than to that for the input values. The root-mean-standard error *RMSE* and the Pearson correlation coefficient (Pearson's *r*) were used to quantify the correction performance. The *RMSE* value of Nanjing is 0.95 kWh/m<sup>2</sup>/day, while Pearson's *r* value is 0.98. That is, the proposed rooftop solar PV potential estimation model has been proven to be very useful.

The initial input solar irradiance was calculated under the assumption of a clear sky with very pure clearness. We use empirical constant to correct the negative influence of actual weather conditions. However, as shown in Fig. 17, there is still a difference between this correction value and the measured surface solar radiation data from the ground observation station. But for the application scenarios of large-scale estimation, this is the result of considering the implementation cost of the method. In future research, we will continue to look for more accurate data to improve the estimation results.

##### 4.2.2. Temporal analysis of the rooftop solar PV potential

This study also conducted a time series analysis of the rooftop solar PV potential in Nanjing and estimated the total rooftop solar PV potential in Nanjing during different periods in 2019 (see Table 6, Fig. 18). In Fig. 18, the hourly rooftop solar PV potential curves are divided into different colors according to the seasonal characteristics of the hourly rooftop solar PV potential: (i) Spring (green): March, April, and May; (ii) Summer (red): June, July, and August; (iii) Autumn (orange): September, October, and November; (iv) Winter (blue): December, January, and February.

Table 6 and Fig. 18 show that the rooftop solar PV potential reaches its maximum value at 11 and 12 a.m. This is because the elevation angle of the sun reaches its maximum value at noon. At this time, the level of direct radiation acceptable to a horizontal receiving surface is highest. It can also be seen in Table 6 and Fig. 18 that the rooftop solar PV potential is highest in May and June. This is because the weather in Nanjing in May and June is mostly clear, and the sun has a higher elevation angle. In contrast, the rooftop solar PV potential is lowest in winter (December, January, and February). In addition, there are different sunrise and sunset times on each day of the year. Therefore, some months receive

Table 6

Total rooftop solar PV potential in Nanjing during different periods of each month in 2019 (GWh).

Month	5–6 a.m.	6–7 a.m.	7–8 a.m.	8–9 a.m.	9–10 a.m.	10–11 a.m.	11 a.m.–12 p.m.	12–1 p.m.	1–2 p.m.	2–3 p.m.	3–4 p.m.	4–5 p.m.	5–6 p.m.	6–7 p.m.	Total
January	0	0	260	931	1653	2218	2525	2522	2206	1629	903	248	0	0	15,094
February	0	23	534	1317	2055	2601	2895	2898	2604	2041	1289	513	19	0	18,789
March	0	167	882	1835	2711	3362	3729	3746	3398	2713	1800	852	147	0	25,342
April	16	473	1353	2318	3160	3770	4105	4127	3816	3194	2330	1354	476	13	30,504
May	125	801	1820	2864	3755	4396	4732	4730	4378	3720	2824	1790	794	101	36,830
June	187	881	1859	2837	3654	4236	4541	4537	4211	3604	2773	1811	868	187	36,186
July	202	935	1864	2748	3483	4007	4283	4284	4006	3470	2719	1824	908	196	34,929
August	73	727	1656	2559	3310	3844	4123	4125	3845	3303	2541	1630	709	27	32,470
September	0	327	1202	2185	3025	3627	3937	3926	3585	2952	2095	1132	307	3	28,303
October	0	54	615	1536	2421	3089	3437	3424	3039	2339	1444	565	28	0	21,991
November	0	0	311	1088	1888	2488	2796	2781	2427	1793	1002	282	3	0	16,860
December	0	0	202	879	1620	2186	2485	2475	2147	1557	821	185	0	0	14,556
Total	602	4388	12,556	23,095	32,734	39,823	43,589	43,576	39,663	32,314	22,540	12,189	4258	526	311,853

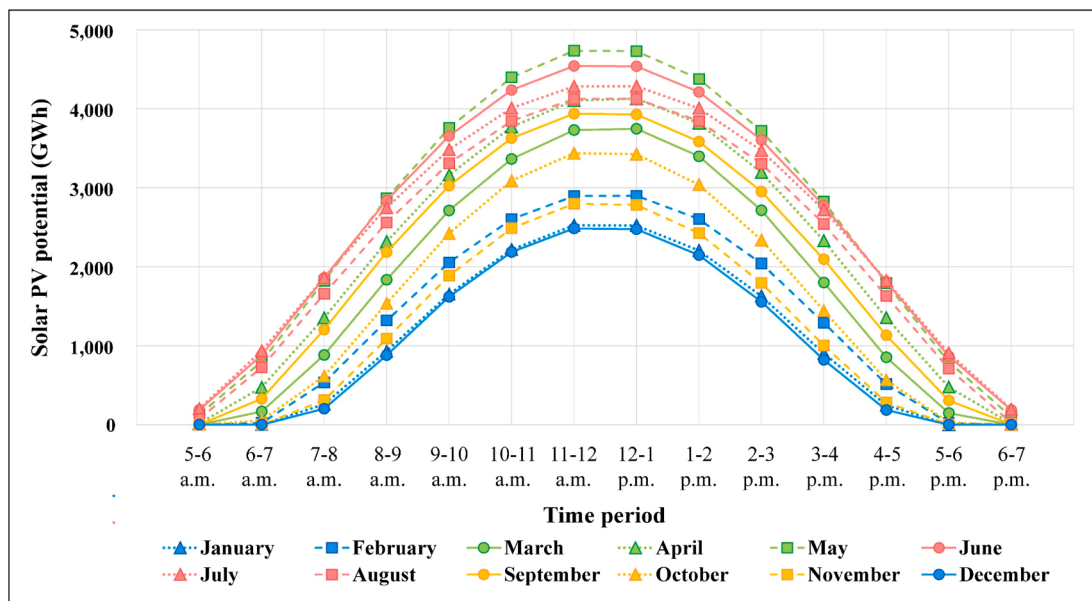


Fig. 18. Rooftop solar PV potential in Nanjing during each month in 2019 (GWh).

zero radiation at 5–7 a.m and 5–7 p.m.

The main city of Nanjing is used as a case study, and the rooftop solar PV potential maps of the four seasons of 2019 were generated (Fig. 19). The total rooftop solar PV potential in downtown Nanjing is 10,690 GWh in spring, 11,948 GWh in summer, 7,746 GWh in autumn, and 5,587 GWh in winter. This result indicates that the rooftop solar PV potential of urban buildings is affected by seasonal changes in solar radiation resources. In spring and summer, the solar altitude angle is large, and the total solar radiation value is high, so the overall rooftop solar PV potential is high in spring and summer. However, the opposite is true in autumn and winter.

#### 4.3. Estimation of the rooftop solar PV power generation

The rooftop solar PV potential estimation is crucial for the accurate measurement of a roof-mounted PV system's installed capacity. To harvest the greatest amount of electricity from a roof-mounted PV system, the PV panels' rated power is selected according to the maximum solar radiation power per hour per unit area of the rooftops in the area. In this study, we calculated that the maximum acceptable solar radiation power per hour per unit area of the rooftop is approximately 400 W. By combining this value with the existing technical conditions, the specification of the solar PV panel is determined to be 1 m × 1 m, and the rated power is 200 W. The total power output of a roof-mounted PV system in Nanjing can be calculated using Eq. (8) [55]:

$$E_P = H_A \cdot \frac{P_{AZ}}{E_s} \cdot K \quad (8)$$

where  $E_P$  is the power generated by solar PV electricity (KWh),  $H_A$  is the annual total solar radiation per unit area,  $P_{AZ}$  is the installed capacity of the solar PV system (KW),  $E_s$  is the standard test condition of photovoltaics (1000 W/m<sup>2</sup>), and  $K$  is the comprehensive efficiency coefficient of the solar PV system, which has a general value of 0.80 [56].

The installed capacity of the solar PV system is calculated from the rated power  $P$  of a single solar PV panel and the number  $N$  of PV panels of a solar PV system using Eq. (9) [57]:

$$P_{AZ} = P \cdot N \quad (9)$$

where  $P$  is the rated power of a single solar PV panel and  $N$  is the number of solar PV panels.

The installed capacity of a roof-mounted PV system and the annual total solar radiation per unit area in Nanjing can be calculated according to the rooftop solar PV power generation estimation method described in Section 4.3 and the rooftop solar PV potential estimation results described in Section 4.2. The measured installed capacity and annual total solar radiation per unit area can then be used to estimate the rooftops' electricity output in Nanjing.

The total rooftop area for installing PV panels is 330.36 km<sup>2</sup>. In this study, the installed solar PV panels have dimensions of 1 m × 1 m and a rated power of 200 W. For the existing urban rooftops, the installed capacity of a roof-mounted PV system was 66 GW, and the annual total solar radiation per unit area was 943.98 KWh/m<sup>2</sup> in 2019. Therefore, the total power output of a roof-mounted PV system based on these urban rooftops was 49,897 GWh for 2019.

The rooftop solar PV power generation's calculation results only represent theoretical design values and do not represent the power generation under actual installation conditions. More factors should be integrated and analyzed to reflect the actual installation situation, such as grid capacity and economic factors. In winter, the peak power of State Grid Nanjing Power Supply Company (the power supply company of Nanjing) is about 10 GW, which is much lower in summer. Nevertheless, the estimated solar PV installed capacity in this study is 66 GW, which is much larger than the grid capacity. However, it is out of this work's scope to model how much solar electricity could be allocated in the power grid. The rooftop is assumed to be a flat surface to reduce the scale of calculations and obtain the final rooftop solar PV power generation. There is a need to further explore the methods to derive the rooftop's slope and aspect information from the satellite images on a city scale when there are no high accurate 3D models of the city.

The transition from fossil fuels to renewable energy is vital to achieving the Paris Agreement's central goal and construct a sustainable future energy system. The growth of solar PV power generation will play a key role in China's energy transition. At present, solar PV power generation in China is facing the policy background of abolishing subsidies altogether. Insightful analysis of rooftop solar PV potential will help the local government promote the future decarbonization

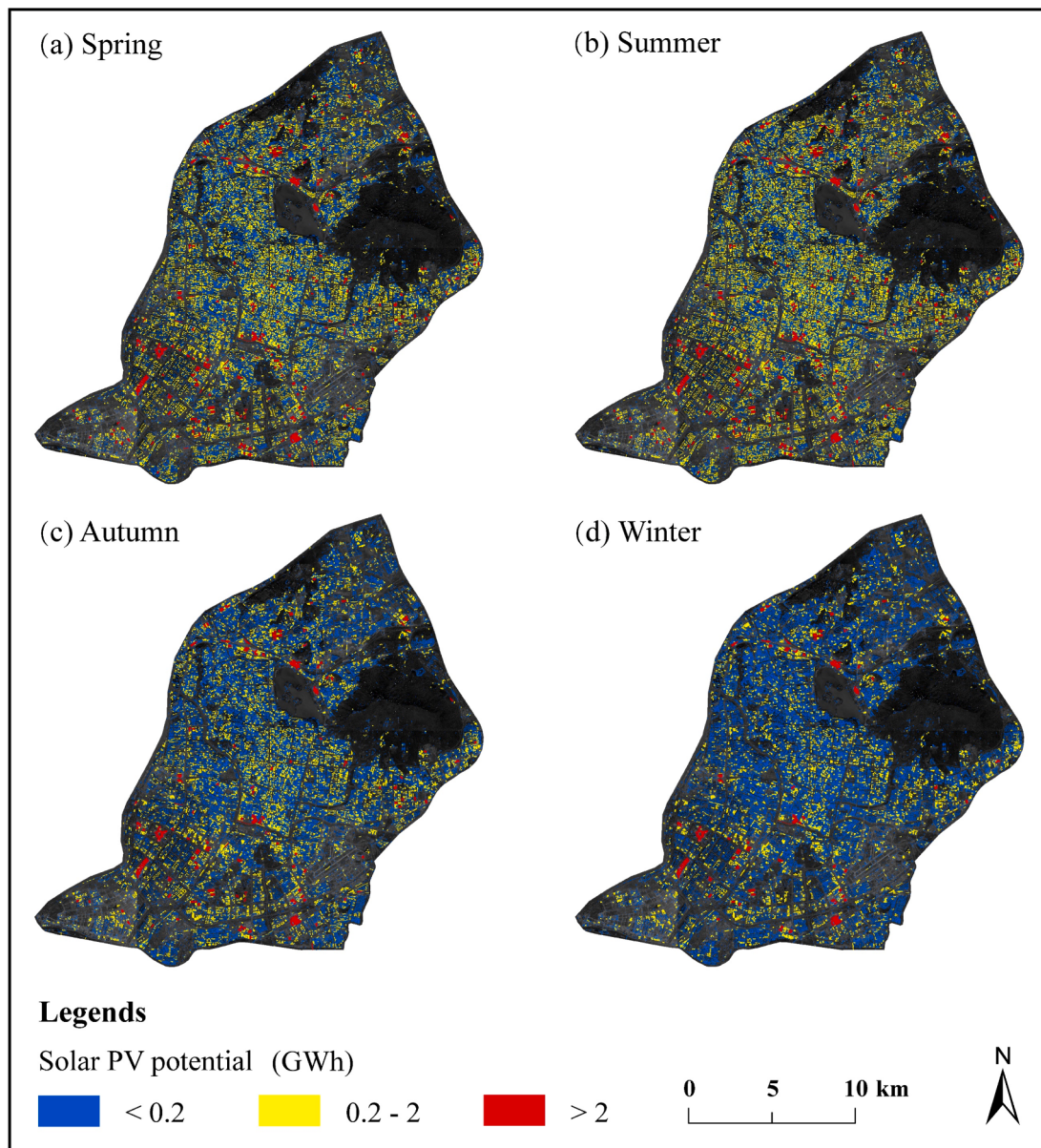


**Fig. 19.** Rooftop solar PV potential in the main city of Nanjing during each season in 2019. (a) Spring, (b) Summer, (c) Autumn, (d) Winter.

transition. According to our experiment results, Nanjing has 330.36 km<sup>2</sup> of rooftop area that can be used to install the distributed solar PV systems. The rooftops of residential buildings accounting for the largest proportion of the rooftop area in Nanjing. There are many high-rise residential buildings in the urban area of Nanjing, which caused difficulties in installing and maintain rooftop solar PV systems. Therefore, it would be more suitable to promote the installation of rooftop solar PV systems in rural areas of Nanjing.

The available area that can be used for installing solar PV panels on rooftops varies greatly in different architectural styles. Taking the 5KW PV power station as an example, PV panels cannot be installed if the available PV area of the rooftop is less than the required 50 square meters. Besides, different architectural styles will directly affect the installation and maintenance costs of solar PV panels. Moderate roof tilt angle is a major factor in installing solar power stations on rooftops. The steep rooftop will affect installation difficulty and result in safety

hazards for installers. Meanwhile, solar PV panels on sloping rooftops are less efficient in generating electricity in summer. The rooftop data extracted in this study is only the rooftop profile and does not contain detailed 3D structure information of the rooftop in terms of slope and aspect. In future research, we will explore the rooftop geometry reconstruction method based on publicly available high-resolution remote sensing image data, which is expected to provide data support for an in-depth analysis of the impact of different architectural styles on solar PV potential.

The influence of building distribution on solar PV potential is mainly on the storage and transport of the generated solar energy. The scientific planning of the location and capacity of the distributed solar PV system is of great significance. Connecting a massive distributed solar PV system to the distribution network will significantly impact the distribution network in terms of voltage level, network loss, and reliability. The degree of influence is closely related to the installation location and

capacity of the distributed solar PV system. In the future study, we will explore the planning of location and capacity of the rooftop solar PV system according to the different distribution modes of urban and rural buildings.

## 5. Conclusions

In this study, a generic method is proposed to estimate the rooftop solar PV potential at the city scale from publicly available GES images. The proposed method is scalable and can be implemented easily in large-scale rooftop solar PV potential estimation with the proposed spatial optimization sampling strategy based on prior knowledge of the urban and rural spatial layout and land use. The available rooftop area is extracted with a deep learning-based image semantic segmentation method. The rooftop solar PV potential and rooftop solar PV power generation in Nanjing are calculated based on the extracted rooftop area. rooftops at the city scale can be extracted from massive satellite images with an accuracy of 0.92 in Nanjing. The estimated annual rooftop solar PV potential in Nanjing is 311,853 GWh, and the rooftop solar PV power generation for 2019 was 49,897 GWh.

The framework developed in this study can extract urban building rooftops without a 3D model, which means that it has high flexibility and can support the rapid promotion of building rooftop solar PV potential assessments in a large-scale study area. With the support of deep learning, image semantic segmentation technology provides strong support for image segmentation refinement. In the future, an image semantic segmentation model with better performance can be further used to improve the performance of the rooftop extraction model. To simplify the estimation, the rooftop is assumed to be a plane in estimating the rooftop solar PV potential. Future studies should consider the influence of the rooftop structure and available area on estimating the PV potential. In addition, the economic cost of deploying a building-attached photovoltaic (BAPV) system is not considered in this study. Future work should evaluate this idea's economic feasibility by comparing the cost of implementing a BAPV system with the potential economic benefits of rooftop solar PV.

## CRediT authorship contribution statement

**Teng Zhong:** Methodology, Investigation, Writing - original draft, Writing - review & editing. **Zhixin Zhang:** Formal analysis, Validation, Data curation, Writing - original draft. **Min Chen:** Conceptualization, Methodology, Writing - review & editing, Project administration, Funding acquisition. **Kai Zhang:** Software, Formal analysis, Data curation. **Zixuan Zhou:** Investigation, Visualization. **Rui Zhu:** Methodology, Writing - review & editing. **Yijie Wang:** Software, Data curation, Visualization. **Guonian Li:** Conceptualization, Writing - review & editing, Supervision. **Jinyue Yan:** Conceptualization, Writing - review & editing, Supervision.

## Declaration of Competing Interest

The authors declare that they have no known competing financial interests or personal relationships that could have appeared to influence the work reported in this paper.

## Acknowledgments

This work was supported by the National Key Research and Development Program of China (Grant 2017YFB0503500), National Research Foundation Singapore.

## Appendix A. Abbreviations and symbols

See Table A1.

**Table A1**  
Abbreviations and symbols.

Abbreviations		Symbols	
PV	Photovoltaic	$GHI_r$	the actual solar radiation received by the horizontal plane
GIS	Geographic Information System	$BHI_h$	the horizontal solar radiation under clear sky conditions
3D	Three-dimensional	$M_t$	the monthly atmospheric transmittance
LiDAR	Light Detection and Ranging	$DHI_h$	the horizontal solar radiation under clear sky conditions
DSM	Digital Surface Model	$M_d$	the monthly diffusion ratio
GES	Google Earth Satellite	$P_{clear}$	the proportion of sunny days in a month
ALS	Airborne Laser Scanning	$P_{cloudy}$	the proportion of cloudy days in a month
OBIA	Object-based Image Analysis	$S_i$	the area of the $i^{th}$ rooftop
SVM	Support Vector Machine	$GHI_{rmdh}$	the corrected real solar radiation between the times $h$ and $h + 1$ in the $m^{th}$ month on the $d^{th}$ day of the year
API	Application Program Interface	$i$	the number of a rooftop ( $i = 1, 2, 3, \dots, n_1$ )
CLAHE	Contrast Limited Adaptive Histogram Equalization	$n_1$	the total number of rooftops
ASPP	Atrous Spatial Pyramid Pooling	$m$	the month ( $m = 1, 2, 3, \dots, 12$ )
BGD	Batch Gradient Descent	$h$	the time in the 24-hour system ( $h = 0, 1, 2, \dots, 23$ )
SGD	Stochastic Gradient Descent	$d$	the day of the month ( $d = 1, 2, 3, \dots, n_2$ )
MBGD	Mini-batch Gradient Descent	$n_2$	the actual number of days per month
CAMS	Copernicus Atmosphere Monitoring Service	$RMSE$	the average difference between the corrected and the observed values
GHI	Global Horizontal Irradiance	$r$	the linear correlation between the corrected and the observed values
BHI	Beam Horizontal Irradiation	$G$	the corrected daily solar irradiance
DHI	Diffuse Horizontal Irradiance	$G_{obs}$	the monthly mean daily solar irradiance observed in a meteorological station
ASR	Annual Solar Radiation	$\bar{G}$	the mean values of the corrected mean daily solar irradiance in the months of a year
DEM	Digital Elevation Model	$\overline{G}_{obs}$	the mean values of the mean daily solar irradiance observed in a meteorological station in the months of a year
BAPV	Building-attached Photovoltaic	$E_p$	the power generated by solar PV electricity (KWh)
		$H_A$	the annual total solar radiation per unit area
		$P_{AZ}$	the installed capacity of the solar PV system (KW)
		$E_s$	the standard test condition of photovoltaics ( $1000 \text{ W/m}^2$ )
		$K$	the comprehensive efficiency coefficient of the solar PV system
		$P$	the rated power of a single solar PV panel
		$N$	the number of solar PV panels

## References

- [1] Duan H-B, Zhang G-P, Zhu L, Fan Y, Wang S-Y. How will diffusion of PV solar contribute to China's emissions-peaking and climate responses? Renew Sustain Energy Rev 2016;53:1076–85. <https://doi.org/10.1016/j.rser.2015.09.021>.
- [2] Tyagi VV, Rahim NAA, Rahim NA, Selvaraj JAL. Progress in solar PV technology: Research and achievement. Renew Sustain Energy Rev 2013;20:443–61. <https://doi.org/10.1016/j.rser.2012.09.028>.
- [3] Zou H, Du H, Ren J, Sovacool BK, Zhang Y, Mao G. Market dynamics, innovation, and transition in China's solar photovoltaic (PV) industry: A critical review. Renew Sustain Energy Rev 2017;69:197–206. <https://doi.org/10.1016/j.rser.2016.11.053>.

- [4] Sun H, Zhi Q, Wang Y, Yao Q, Su J. China's solar photovoltaic industry development: The status quo, problems and approaches. *Appl Energy* 2014;118: 221–30. <https://doi.org/10.1016/j.apenergy.2013.12.032>.
- [5] Xu M, Xie P, Xie B-C. Study of China's optimal solar photovoltaic power development path to 2050. *Resour Policy* 2020;65. <https://doi.org/10.1016/j.respol.2019.101541>.
- [6] Yan J, Yang Y, Elia Campana P, He J. City-level analysis of subsidy-free solar photovoltaic electricity price, profits and grid parity in China. *Nat Energy* 2019;4: 709–17. <https://doi.org/10.1038/s41560-019-0441-z>.
- [7] International Energy Agency (IEA). Prospects for distributed energy systems in China, <https://www.iea.org/reports/prospects-for-distributed-energy-systems-in-china> [accessed 15 August 2020].
- [8] Zhao X-G, Zhen W. Technology, cost, economic performance of distributed photovoltaic industry in China. *Renew Sustain Energy Rev* 2019;110:53–64. <https://doi.org/10.1016/j.rser.2019.04.061>.
- [9] Brito MC, Freitas S, Guimarães S, Catita C, Redweik P. The importance of facades for the solar PV potential of a Mediterranean city using LiDAR data. *Renewable Energy* 2017;111:85–94. <https://doi.org/10.1016/j.renene.2017.03.085>.
- [10] Rigter J, Vidican G. Cost and optimal feed-in tariff for small scale photovoltaic systems in China. *Energy Policy* 2010;38:6989–7000. <https://doi.org/10.1016/j.enpol.2010.07.014>.
- [11] Jia X, Du H, Zou H, He G. Assessing the effectiveness of China's net-metering subsidies for household distributed photovoltaic systems. *J Cleaner Prod* 2020;262. <https://doi.org/10.1016/j.jclepro.2020.121161>.
- [12] Assouline D, Mohajeri N, Scartezzini JL. Quantifying rooftop photovoltaic solar energy potential: A machine learning approach. *Sol Energy* 2017;141:278–96. <https://doi.org/10.1016/j.solener.2016.11.045>.
- [13] Liang J, Gong J, Li W. Applications and impacts of Google Earth: A decadal review (2006–2016). *ISPRS J Photogramm Remote Sens* 2018;146:91–107. <https://doi.org/10.1016/j.isprsjprs.2018.08.019>.
- [14] Qi F, Wang Y. A new calculation method for shape coefficient of residential building using Google Earth. *Energy Build* 2014;76:72–80. <https://doi.org/10.1016/j.enbuild.2014.02.058>.
- [15] Shi Y, Li Q, Zhu X-X. Building segmentation through a gated graph convolutional neural network with deep structured feature embedding. *ISPRS J Photogramm Remote Sens* 2020;159:184–97. <https://doi.org/10.1016/j.isprsjprs.2019.11.004>.
- [16] Huang Z, Mendis T, Xu S. Urban solar utilization potential mapping via deep learning technology: A case study of Wuhan, China. *Appl Energy* 2019;250: 283–91. <https://doi.org/10.1016/j.apenergy.2019.04.113>.
- [17] Werkhoven BV, Maassen J, Bal HE, Seinstra FJ. Optimizing convolution operations on GPUs using adaptive tiling. *Future Generat Comput Syst* 2014;30:14–26. <https://doi.org/10.1016/j.future.2013.09.003>.
- [18] Mittal S, Vaishay S. A survey of techniques for optimizing deep learning on GPUs. *J Syst Archit* 2019;99. <https://doi.org/10.1016/j.jysarc.2019.101635>.
- [19] Mittal S. A Survey on optimized implementation of deep learning models on the NVIDIA Jetson platform. *J Syst Archit* 2019;97:428–42. <https://doi.org/10.1016/j.jysarc.2019.01.011>.
- [20] Zhang Y, Ren J, Pu Y, Wang P. Solar energy potential assessment: A framework to integrate geographic, technological, and economic indices for a potential analysis. *Renewable Energy* 2020;149:577–86. <https://doi.org/10.1016/j.renene.2019.12.071>.
- [21] Schallenberg-Rodríguez J. Photovoltaic techno-economic potential on roofs in regions and islands: The case of the Canary Islands. Methodological review and methodology proposal. *Renew Sustain Energy Rev* 2013;20:219–39. <https://doi.org/10.1016/j.rser.2012.11.078>.
- [22] Wigington LK, Nguyen HT, Pearce JM. Quantifying rooftop solar photovoltaic potential for regional renewable energy policy. *Comput Environ Urban Syst* 2010; 34:345–57. <https://doi.org/10.1016/j.compenvurbsys.2010.01.001>.
- [23] Izquierdo S, Rodrigues M, Fueyo N. A method for estimating the geographical distribution of the available roof surface area for large-scale photovoltaic energy-potential evaluations. *Sol Energy* 2008;82:929–39. <https://doi.org/10.1016/j.solener.2008.03.007>.
- [24] Hong T, Lee M, Koo C, Jeong K, Kim J. Development of a method for estimating the rooftop solar photovoltaic (PV) potential by analyzing the available rooftop area using Hillshade analysis. *Appl Energy* 2017;194:320–32. <https://doi.org/10.1016/j.apenergy.2016.07.001>.
- [25] Levinson R, Akbari H, Pomerantz M, Gupta S. Solar access of residential rooftops in four California cities. *Sol Energy* 2009;83:2120–35. <https://doi.org/10.1016/j.solener.2009.07.016>.
- [26] Ko L, Wang J-C, Chen C-Y, Tsai H-Y. Evaluation of the development potential of rooftop solar photovoltaic in Taiwan. *Renewable Energy* 2015;76:582–95. <https://doi.org/10.1016/j.renene.2014.11.077>.
- [27] Mainzer K, Fath K, McKenna R, Stengel J, Fichtner W, Schultmann F. A high-resolution determination of the technical potential for residential-roof-mounted photovoltaic systems in Germany. *Sol Energy* 2014;105:715–31. <https://doi.org/10.1016/j.solener.2014.04.015>.
- [28] Gagnon P, Margolis R, Melius J, Phillips C, Elmore R. Rooftop solar photovoltaic technical potential in the United States. A detailed assessment; 2016. <https://www.osti.gov/servlets/purl/1236037>.
- [29] Hosseini SE. Development of solar energy towards solar city Utopia. *Energy Sources Part A* 2019;41:2868–81. <https://doi.org/10.1080/15567036.2019.1576803>.
- [30] Freitas S, Catita C, Redweik P, Brito MC. Modelling solar potential in the urban environment: State-of-the-art review. *Renew Sustain Energy Rev* 2015;41:915–31. <https://doi.org/10.1016/j.rser.2014.08.060>.
- [31] Liu Z, Yang A, Gao M, Jiang H, Kang Y, Zhang F, et al. Towards feasibility of photovoltaic road for urban traffic-solar energy estimation using street view image. *J Cleaner Prod* 2019;228:303–18. <https://doi.org/10.1016/j.jclepro.2019.04.262>.
- [32] De Schepper E, Van Passel S, Manca J, Thewys T. Combining photovoltaics and sound barriers – A feasibility study. *Renewable Energy* 2012;46:297–303. <https://doi.org/10.1016/j.renene.2012.03.022>.
- [33] Gooding J, Crook R, Tomlin AS. Modelling of roof geometries from low-resolution LiDAR data for city-scale solar energy applications using a neighbouring buildings method. *Appl Energy* 2015;148:93–104. <https://doi.org/10.1016/j.apenergy.2015.03.013>.
- [34] Hoferka J, Zlocha M. A new 3-D solar radiation model for 3-D City Models. *Trans GIS* 2012;16:681–90. <https://doi.org/10.1111/j.1467-9671.2012.01337.x>.
- [35] Jakubiec JA, Reinhardt CF. A method for predicting citywide electricity gains from photovoltaic panels based on LiDAR and GIS data combined with hourly Daysim simulations. *Sol Energy* 2013;93:127–43. <https://doi.org/10.1016/j.solener.2013.03.022>.
- [36] Mohajeri N, Assouline D, Guiboud B, Bill A, Gudmundsson A, Scartezzini J-L. A city-scale roof shape classification using machine learning for solar energy applications. *Renewable Energy* 2018;121:81–93. <https://doi.org/10.1016/j.renene.2017.12.096>.
- [37] Romero Rodríguez L, Duminil E, Sánchez Ramos J, Eicker U. Assessment of the photovoltaic potential at urban level based on 3D city models: A case study and new methodological approach. *Sol Energy* 2017;146:264–75. <https://doi.org/10.1016/j.solener.2017.02.043>.
- [38] Redweik P, Catita C, Brito M. Solar energy potential on roofs and facades in an urban landscape. *Sol Energy* 2013;97:332–41. <https://doi.org/10.1016/j.solener.2013.08.036>.
- [39] Li Y, Ding D, Liu C, Wang C. A pixel-based approach to estimation of solar energy potential on building roofs. *Energy Build* 2016;129:563–73. <https://doi.org/10.1016/j.enbuild.2016.08.025>.
- [40] Jochem A, Höfle B, Rutzinger M, Pfeifer N. Automatic roof plane detection and analysis in airborne lidar point clouds for solar potential assessment. *Sensors (Basel)* 2009;9:5241–62. <https://doi.org/10.3390/s90705241>.
- [41] Aguiar G, Nex F, Remondino F, Filippi RD, Droghetti S, Furlanello C. Solar radiation estimation on building roofs and web-based solar cadaster. *Remote Sens Spatial Inf Sci* 2013. <https://doi.org/10.5194/isprsaannals-1-2-177-2012>.
- [42] Kabir MH, Endlicher W, Jägermeyr J. Calculation of bright rooftops for solar PV applications in Dhaka Megacity, Bangladesh. *Renewable Energy* 2010;35:1760–4. <https://doi.org/10.1016/j.renene.2009.11.016>.
- [43] Huang J, Zhang X, Xin Q, Sun Y, Zhang P. Automatic building extraction from high-resolution aerial images and LiDAR data using gated residual refinement network. *ISPRS J Photogramm Remote Sens* 2019;151:91–105. <https://doi.org/10.1016/j.isprsjprs.2019.02.019>.
- [44] Nanjing Bureau of Statistics. Nanjing statistical yearbook 2019. Beijing: China Statistics Press; 2019.
- [45] Li M, Huang C, Shen W, Ren X, Lv Y, Wang J, et al. Characterizing long-term forest disturbance history and its drivers in the Ning-Zhen Mountains, Jiangsu Province of eastern China using yearly Landsat observations (1987–2011). *J For Res* 2016; 27:1329–41. <https://doi.org/10.1007/s11676-016-0262-x>.
- [46] Xiong Y, Liu J, Kim J. Understanding differences in thermal comfort between urban and rural residents in hot summer and cold winter climate. *Build Environ* 2019; 165:106393–403. <https://doi.org/10.1016/j.buildenv.2019.106393>.
- [47] Nanjing Bureau of Natural Resources and Planning. Nanjing urban master plan (2011–2020), [http://ghj.nanjing.gov.cn/ghbz/ztgh/201705/t20170509\\_874089.html](http://ghj.nanjing.gov.cn/ghbz/ztgh/201705/t20170509_874089.html) [accessed 15 August 2020].
- [48] Mi L, Chen Z. Superpixel-enhanced deep neural forest for remote sensing image semantic segmentation. *ISPRS J Photogramm Remote Sens* 2020;159:140–52. <https://doi.org/10.1016/j.isprsjprs.2019.11.006>.
- [49] Zhu D, Xia S, Zhao J, Zhou Y, Jian M, Niu Q, et al. Diverse sample generation with multi-branch conditional generative adversarial network for remote sensing objects detection. *Neurocomputing* 2020;381:40–51. <https://doi.org/10.1016/j.neucom.2019.10.065>.
- [50] El Mghouchi Y, El Bouardi A, Choulli Z, Ajzoul T. New model to estimate and evaluate the solar radiation. *Int J Sustain Built Environ* 2014;3:225–34. <https://doi.org/10.1016/j.ijsbe.2014.11.001>.
- [51] Yoshida S, Ueno S, Kataoka N, Takakura H, Minemoto T. Estimation of global tilted irradiance and output energy using meteorological data and performance of photovoltaic modules. *Sol Energy* 2013;93:90–9. <https://doi.org/10.1016/j.solener.2013.04.001>.
- [52] Huang S, Rich PM, Crabtree RL, Potter CS, Fu P. Modeling monthly near-surface air temperature from solar radiation and lapse rate: application over complex terrain in yellowstone national park. *Phys Geogr* 2013;29:158–78. <https://doi.org/10.2747/0272-3646.29.2.158>.

- [53] Kodysh JB, Omitaomu OA, Bhaduri BL, Neish BS. Methodology for estimating solar potential on multiple building rooftops for photovoltaic systems. Sustain Cities Soc 2013;8:31–41. <https://doi.org/10.1016/j.scs.2013.01.002>.
- [54] Zamir AR, Wekel T, Argawal P, Weil C, Malik J, Savarese S. Generic 3D representation via pose estimation and matching. Eur Conf Comput Vision 2016. [https://doi.org/10.1007/978-3-319-46487-9\\_33](https://doi.org/10.1007/978-3-319-46487-9_33).
- [55] Ministry of Housing and Urban-Rural Construction of the People's Republic of China. China code for design of photovoltaic power station. Beijing: Standards Press of China; 2012.
- [56] Berwal AK, Kumar S, Kumari N, Kumar V, Haleem A. Design and analysis of rooftop grid tied 50 kW capacity Solar Photovoltaic (SPV) power plant. Renew Sustain Energy Rev 2017;77:1288–99. <https://doi.org/10.1016/j.rser.2017.03.017>.
- [57] Qi L, Jiang M, Lv Y, Yan J. A celestial motion-based solar photovoltaics installed on a cooling tower. Energy Convers Manage 2020;216:112957–69. <https://doi.org/10.1016/j.enconman.2020.112957>.